electronics

MDPI

Review

A Recent Approach towards Fluidic Microstrip Devices and Gas Sensors: A Review

Suleiman Aliyu Babale [1], Kashif Nisar Paracha [2], Sarosh Ahmad [2,3,*], Sharul Kamal Abdul Rahim [4], Zainab Yunusa [1], Muhammad Nasir [5], Adnan Ghaffar [6,*] and Abdenasser Lamkaddem [3]

1 Department of Electrical Engineering, Bayero University Kano–Nigeria, Kano 700006, Nigeria; sababale.ele@buk.edu.ng (S.A.B.); zyyusuf.ele@buk.edu.ng (Z.Y.)
2 Department of Electrical Engineering and Technology, Government College University Faisalabad (GCUF), Faisalabad 38000, Pakistan; kashifnisar@gcuf.edu.pk
3 Department of Signal Theory and Communications, Universidad Carlos III de Madrid, 28911 Madrid, Spain; alamkadd@ing.uc3m.es
4 Wireless Communication Centre, School of Electrical Engineering, Universiti Teknologi Malaysia (UTM), Skudai 81310, Malaysia; sharulkamal@fke.utm.my
5 Electrical Engineering Department, Faisalabad Campus, University of Engineering and Technology Lahore (UET, Lahore), Faisalabad 38000, Pakistan; muhammad.nasir@uet.edu.pk
6 Department of Electrical and Electronic Engineering, Auckland University of Technology, Auckland 1010, New Zealand
* Correspondence: saroshahmad@ieee.org (S.A.); aghaffar@aut.ac.nz (A.G.)

Abstract: This paper aims to review some of the available tunable devices with emphasis on the techniques employed, fabrications, merits, and demerits of each technique. In the era of fluidic microstrip communication devices, versatility and stability have become key features of microfluidic devices. These fluidic devices allow advanced fabrication techniques such as 3D printing, spraying, or injecting the conductive fluid on the flexible/rigid substrate. Fluidic techniques are used either in the form of loading components, switching, or as the radiating/conducting path of a microwave component such as liquid metals. The major benefits and drawbacks of each technology are also emphasized. In this review, there is a brief discussion of the most widely used microfluidic materials, their novel fabrication/patterning methods.

Keywords: microfluidic devices; reconfigurable filters; fluidic couplers; power dividers; phase shifters; SPST switches; MEMS switches

Citation: Babale, S.A.; Paracha, K.N.; Ahmad, S.; Abdul Rahim, S.K.; Yunusa, Z.; Nasir, M.; Ghaffar, A.; Lamkaddem, A. A Recent Approach towards Fluidic Microstrip Devices and Gas Sensors: A Review. *Electronics* **2022**, *11*, 229. https://doi.org/10.3390/electronics11020229

Academic Editor: Daniel Gutiérrez Reina

Received: 16 November 2021
Accepted: 17 December 2021
Published: 12 January 2022

1. Introduction

Over the past decade, switchable/tunable microwave components have become an active research area, and much research reveals that tunable microwave components can improve the performances of RF and microwave devices in many ways. Improvements in the frequency of tunable devices, such as microelectromechanical systems (MEMS) [1–4], field-effect transistor (FET) couplers, power dividers, phase shifters, filters, sensors, switches [5,6] varactor diodes [7–10], and PIN diodes [11–14], permitted the popularity of frequency-switchable technologies, leading to versatility and reliability of the systems. Despite many of the advantages of tunable devices, such as fast switching, improvement in bandwidth, and high quality they offered, these tunable mechanisms, on the other hand, have some drawbacks. They have poor power-handling capability and are not fully compatible with many conformal devices. They also required DC bias networks to function. However, it is quite challenging to isolate the control circuitry and the biasing network [15]. For tunable microwave components to be compatible with conformal devices, the passive components associated with it also be to be flexible as well. This implies that it will be difficult to use the classical printed circuit board printing technologies for prototyping such components. To find better ways for prototyping such flexible components incorporated with tunable

circuitries, it is necessary to make use of various techniques of using fluidics within the microwave components to have full flexibility of the devices.

Fluidic techniques are used either in the form of loading components, switching, or as the radiating/conducting path of a microwave component such as liquid metals. In either case, they have to gain more popularity because of their benefits compared to semiconductor devices ad MEMS [16]. Some of these advantages are its low insertion loss, high linearity, high radiation efficiency, high-frequency tunability, and easy fabrication compared with other tuning and switching approaches [17]. Due to its tremendous advantages, the microfluidic technique is becoming an alternative switching method due to the fact that it does not require any separate DC biasing networks [18]. This proposed paper aims to review some of the available tunable devices with emphasis on the techniques employed, fabrications, merits, and demerits of each technique to guide researchers working in the area.

2. Fluidic Coupler, Power Divider, and Phase Shifters

A quad-port coupler is a uniform network to when any of the coupler's port is excited with power, then it divides the power correspondingly among the two opposing ports with one of the outputs lagging the other by 90°, whereas the next port to the input is fully separated. A fluidically tunable branchline coupler (BLC) was presented in [19]. In this design, a classical BLC was designed, and the ground path was etched, forming 12 channels beneath the main structure of the BLC, as shown in Figure 1. To evaluate the frequency-tuning response of the coupler, these channels were systematically occupied with the $C_4H_8O_2$ (dielectric-fluid-ethyl-acetate).

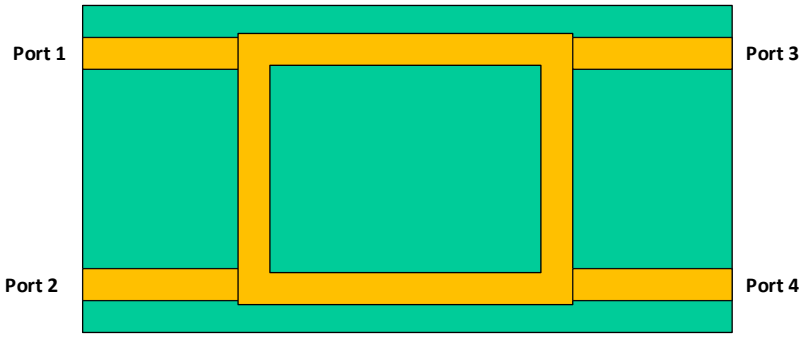

Figure 1. Diagram of the tunable branch line coupler (BLC).

The dielectric and loss tangents of the fluid are 6.0 and 0.0059, correspondingly. From the fluid's dielectric property, it could be observed that the difference between the substrate's permittivity and that of the fluid is almost the same as the difference between that of the substrate and air. For this reason, both the ascending and the descending frequency shift of the coupler when the four channels are completely or partially filled with the fluid, and when it is empty, then it is almost comparative to the operating frequency of the coupler. After forming the channels, two cases were considered. The first case is when no fluid is injected into the coupler. The second case is when the fluid is injected onto the coupler. In this latter case, it was injected such that the symmetrical nature of the coupler is maintained. In both cases, the coupler was measured by means of VNA (vector network analyzer) from 1 to 3 GHz. The experimental results have shown an excellent tuning of about 390 MHz within the range from 2.19 to 1.80 GHz. Microwave power dividers, on the other hand, are cousin brothers to hybrid couplers with little difference in the number of ports and the output phase difference. It plays a significant role in microwave devices. It is a network whose input power is divided into N-ways output according to some proportions. A microfluidic compact broadband power divider was designed and implemented in [20] using nematic liquid crystal. In this paper, the power divider used an inverted microstrip line and loaded a split-ring resonator (SRR) on the metal conduction band. It also loads

a nematic liquid crystal on the inverted microstrip lines, which results in providing a wideband power divider operating in C band.

The major setback of using nematic liquid crystal is that the arrangement of its molecular structure is not as stable compared to its crystal form. As such, it is susceptible to variation because of environmental changes such as temperature and the presence of electromagnetic fields.

Phase shifters are an important part of the building block of many wireless mobile communications equipment. It is a gadget that provides a variation in the phase angle of each signal that travels across it. Favorably, it must not yield any attenuation, and it must be excellently equal from input to the output terminal of the transmission line. In the case of the microstrip method, any further line in addition to a recommended line presents a phase shift [21]. A reconfiguration phase shifter presented in [22] is also based on a microfluidic technique. It consists of a conventional coupler with reflective microstrip lines at the terminations ends. From this design setup, a microfluidic channel is constructed with a polydimethylsiloxane (PDMS) layer, and the selectively metalized plate (SMP) prepared from Rogers RO4003C was sandwiched in-between the microfluidic and the reflective microstrip terminations line to vary the electrical lengths of the main phase shifter through the capacitive short mechanism. Figure 2 depicts the prototype and the return loss results presenting the insertion and return losses exhibited by the reconfiguration phase shifter. The design comprehends 360-degree phase difference with an overall 9.5 mm SMP shift subsequently given a total actuation time of 1.95 s with the micropumps. However, insertion and return loss better than 20 and 0.95 dB, respectively, were achieved in the whole-frequency bands.

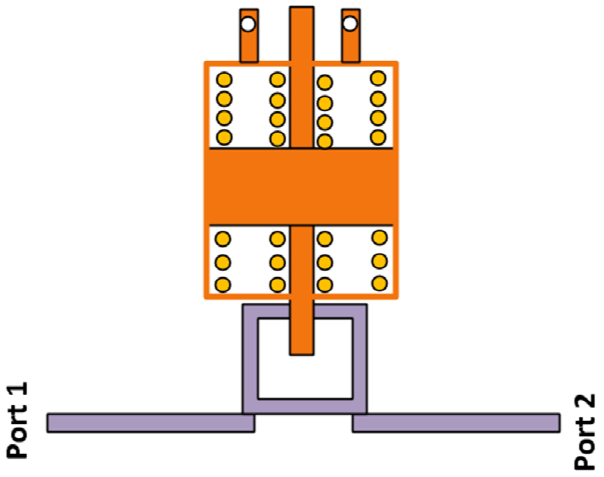

Figure 2. The photograph of the phase-shifter.

A 4 × 4 Butler matrix using single-layered Rogers' RO3003 substrate without phase shifters is reported in [23]. A dual-band novel BLC (branchline coupler) and a 4 × 4 Butler matrix with modified PI-shaped TL are reported in [24]. The proposed novel BLC is a dual resonance branchline coupler and combination of the phase shifter and able to accomplish dual-band resonance for 2.3–4.4 frequency ratios. In both cases, the prototypes were calculated by means of a VNA from 1 to 3 GHz. Roger 5870 with relative permittivity of ε_r = 2.33, tangent loss of tan δ = 0.0012, and thickness of h = 0.787 mm is used as a substrate. The S11- features of the projected dual resonance branchline coupler (BLC) achieved the maximum phase-deviation and amplitude imbalance of about and respectively. Figure 3 depicts the prototype of BLC and 4 × 4 BM and simulated and measured phase difference in degrees.

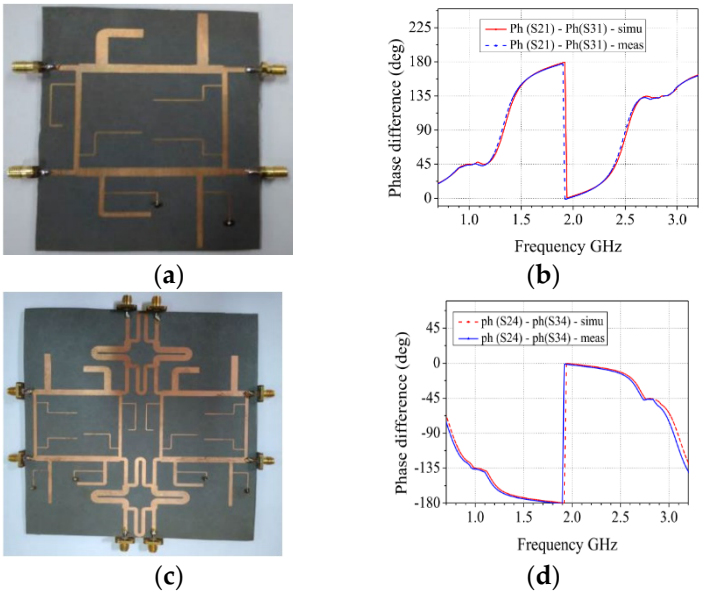

Figure 3. (**a**) The branchline coupler (BLC) prototype; (**b**) simulated measured phase variation of BLC; (**c**) the 4 × 4 Butler matrix prototype; (**d**) measured and simulated phase difference of 4 × 4 Butler matrix [24].

On the other hand, a compact size UWB 90-degree phase shifter is designed in [25]. It consists of a main line and a reference line to make it ultra-wideband. This miniaturized phase-shifter covers the frequency range from 1.36 to 4.53 GHz with only ±5% phase error. Roger RO4350B with epsilon value of ε_r = 3.48, tangent loss tan δ = 0.0037, and a height of h = 0.762 mm is used as a substrate. Figure 4 depicts the miniaturized phase shifter and shifted phase results exhibited by the UWB phase shifter. However, a return loss and insertion loss superior to 1.25 and 20 dB, correspondingly, were achieved in the whole-frequency bands.

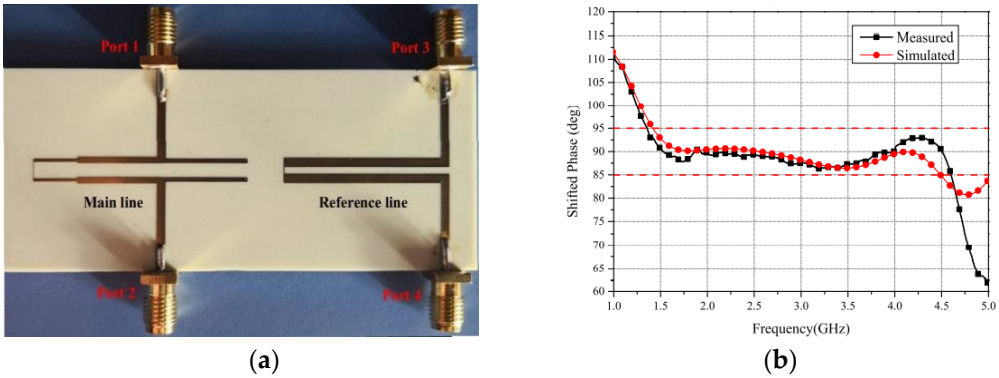

Figure 4. (**a**) The UWB phase shifter; (**b**) simulated and measured performance of the phase shifter [25].

An inkjet printer 3 dB coupler with flexible phase difference and equal power division is presented in the work of [26]. This 3 dB coupler covers the frequency range from 5.09 to 6.97 GHz with a slight phase variation of about ±1°. Transparent polyethylene terephthalate (PET) with epsilon in free space ε_r = 2.71, tan δ = 0.043 (loss tangent), and h = 0.125 mm (thickness) is used as a substrate. Figure 5 depicts the 3 dB coupler with simulated and measured results. However, a return loss and insertion loss are −28 and −48 dB, respectively, and were achieved in the whole-frequency bands. The overview about the fluid coupler, power divider, and phase shifters is given in Table 1.

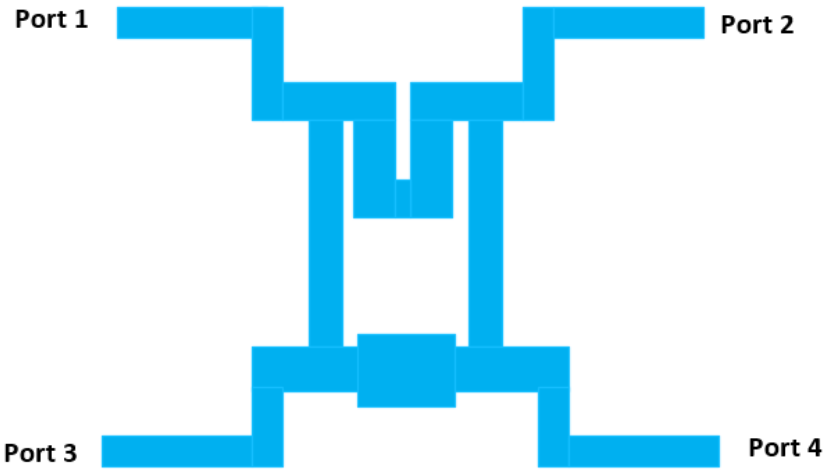

Figure 5. A picture of the 3 dB branchline coupler.

Table 1. Comparison analysis of fluidic coupler, power divider, and phase shifters.

References	Fluid Material/Substrate	Technique/Type	Band	Application	Advantage	Disadvantage
[19]	Rogers' RO4003	Tunable branchline coupler	1.8–2.29 GHz	Microfluidic application	Reconfigurability/power combiner/simple design	Need to improve the errors, coupler mismatching
[20]	Nematic liquid crystal	Inverted microstrip line with loaded split-ring resonator (SRR)	C band	Power coupler	Low loss, easy integration with other circuits RL > 24 dB IL = 3 dB	Susceptible to environment change and EM radiation
[21]	Polyethylene terephthalate (PET)	Low-cost inkjet printing technique	6 GHz	Phase shifters/4 × 4 Butler matrix (BM) for wearable applications	High isolation and return loss/RL. 19 dB IL. 0 dB 90-degree phase shifted	Susceptible to environment change and EM radiation
[22]	PDMS and SMP prepared from Rogers RO4003C sandwiched in b/w microfluidic and the reflective microstrip terminations line	Microfluidic techniques	x-band	Microfluidically reconfigurable reflection phase shifter	Low loss and high power-handling capability/360° phase shifted, RL. 20 dB, IL. 0.95 dB	Not miniaturized/susceptible to environment change and EM radiation
[23]	Rogers' RO3003	Microstrip hybrid modified coupler	6 GHz	4-by-4 Butler matrix for future 5G	Stable beam-scanning, Couplers having 45° Phase difference/ RL: 25.6 dB 45° PS	Complex issues involved in the design of Butler matrix
[24]	Rogers 5870	Modified PI-shaped transmission lines (TL)	1 and 2.85 GHz	Dual-band branchline coupler and 4 × 4 Butler matrix	Compact size, simple design,	Not UWB/large size/Susceptible to environment change and EM radiation
[25]	RO4350B substrate	Miniaturization	1.36 to 4.53 GHz	Phase shifter used in mobile communication systems	Compatible to integrated communication systems./Suitable agreement with the EM simulation/ultrawideband/ miniaturized/ RL. 20 dB, IL. 1.25 dB	-
[26]	Transparent polyethylene terephthalate (PTE)	Instant inkjet printing silver nano	5.09 to 6.97 GHz	Inkjet-printed 3 dB coupler	Fast prototyping of electronic circuitries RL = −28 dB	Narrowband/susceptible to environment change and EM radiation

3. Microfluidic Reconfigurable Filters

Fluidic channels are used in microwave circuits for unlike applications such as reconfiguration, polarization, and frequency tuning. In this sub-heading, different methods for reconfigurable filters are mainly discussed. Reference [27] proposed a substrate concentrated of the microfluidically reconfigured frequency-tunable filter as depicted in Figure 6.

In this setup, Rogers 6010 substrate with peak relative permittivity and tangent loss of ε_r = 10.2 and tan δ = 0.0025 correspondingly, is used for the recognition of the microstrip line resonators. The second substrate was formed from PDMS, having dielectric and loss tangents of 2.8 and 0.04 individually. The microfluidic channel is created on the PDMS, and the two substrates were bonded by means of benzo cyclobutene (BCB) having ε_r = 2.4 and tan δ = 0.002. With the aid of a metal plate (MP), a less lossy dielectric fluid 3 M FC-40 with density = 1.855 g/cm^3, tan δ = 0.0005, and ε_r = 1.9 was used to fill the channel created. The results obtained revealed that the unpacked Q.F. (quality factor) of the resonators is sustained a dielectric constant value within 210 to 190 across the whole tunable range with a very less insertion loss (IL = 3 dB) and a greater power-handling capacity of about 15 W under continuous excitation of the power. A fractional bandwidth of the filter design was experimentally verified to be about 5%.

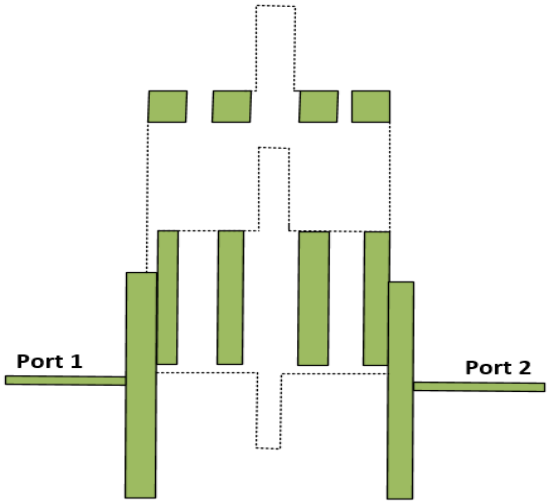

Figure 6. Microfluidically reconfigurable half-wavelength resonator filter.

A microfluidic reconfigurable triple-band filter resonating at (1, 1.4, and 1.8) GHz was designed and presented in [28]. The structure was constructed by means of dual-mode ring resonators, and the metallic liquid switches were used inside for the interrelation of various resonators and lines. The design employed eutectic gallium indium liquid metal as the fluid mixed up with sodium hydroxide for improvement in the liquid metal fluidity. The combination of these fluids is used as the switches for shifting different frequencies, and micropumps are used to inject the liquid metal switches. This configuration has the advantage of providing autonomous exterior Q tuning that is obtained by converting means of various tap coupling feedlines. This design was printed on a Rogers UL200 substrate with ε_r = 2.5 and a height of h = 0.762 mm, as shown in Figure 7. Fairly suitable experimental insertion losses at the three bands were found to be 0.68, 0.69, and 0.47 dB, respectively.

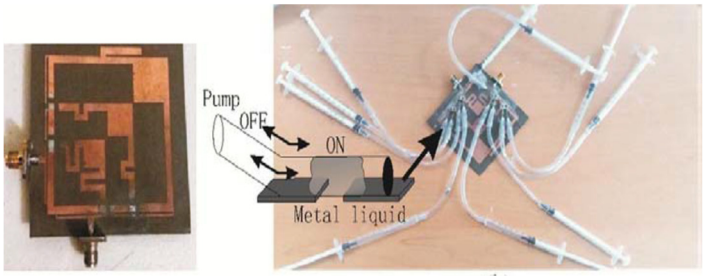

(a) **(b)**

Figure 7. (**a**) Prototype fabricated filter; (**b**) setup of filter presenting a schematic of the metallic switch and a figure of the final setup with syringes used as micropumps [28].

A bandpass filter operating at dual-band frequencies with fixed lower-frequency band and tunable higher-frequency band was presented in [29]. This paper consists of a microfluidic channel, stub, and two split-ring resonators (SRRs). The resonant frequency at the lower band is being controlled by one of the SRR, whereas the combination of the stub and the other SRR-controlled the upper frequency. However, the higher band is being resolved by stub lengths and the SRR. A metallic liquid called EGaIn (eutectic gallium indium) includes indium that is being inserted into the microfluidic channel to excellently change the electrical stub length. The channel was melded from polydimethylsiloxane (PDMS) elastomer. Figure 8a proves the area of the setup, and the picture of the prototype filter is shown in Figure 8b.

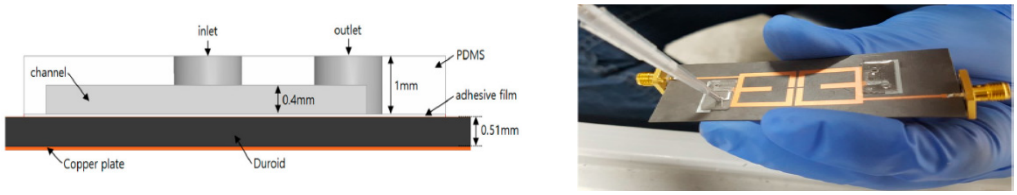

Figure 8. (**a**) Side view of the final filter; (**b**) pictures of the proposed prototype filter injecting EGaIn into the filter [29].

The fluidic channel was fabricated with the aid of a 3D printer, and the complete filter was printed on a flexible Rogers substrate RT5880 with ε_r = 2.2, as presented in Figure 8. When the metallic liquid was inserted into the channel, the result of the EGaIn enlarging the dimension of the stub, and this, in turn, reduces the resonance band. This variation in frequency is depicted in Figure 9. From the results of the transmission coefficient obtained, the lower band was kept fixed at 1.85 GHz, but the upper band was kept movable from 2.95 to 3.06 GHz as a result of injecting the liquid metal into the channels.

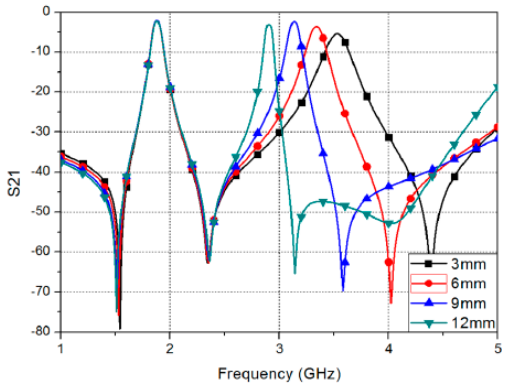

Figure 9. Transmission coefficient of the proposed filter for different stub length Ls [29].

One of the common challenges of using polydimethylsiloxane (PDMS) is how to bond it with a different material. In this case, the adhesive film used to bond the Rogers substrate and the PDMS together might be responsible for the slide shift at the upper resonance frequency [30]. A frequency-reconfigurable CSRR (complementary-split-ring-resonator) loaded QMSIW (quarter-mode-substrate-integrated-waveguide) bandpass filter was presented in [31], Other fluidically based microwave devices are reflection-type oscillators using a SIW (substrate-integrated-waveguide) resonator [32], microfluidically controlled waveguide switch [33], and fluidic split-ring resonator [34]. The proposed fluidic bandpass filter, CSRR, was formed as a square-shaped slot design divided in the metallic pattern. Once the complementary split-ring resonator is overloaded on the upper level of the QMSIW structure, it results in tremendous size reduction in the structure, which directly

provides advantages in terms of cost and space conservation. For frequency switchability, a microfluidic channel with a PDMS substrate and EGaIn was used. It is printed by using the 3D printer. Figure 10 illustrates the prototype method of the microfluidic channel with a PDMS substrate.

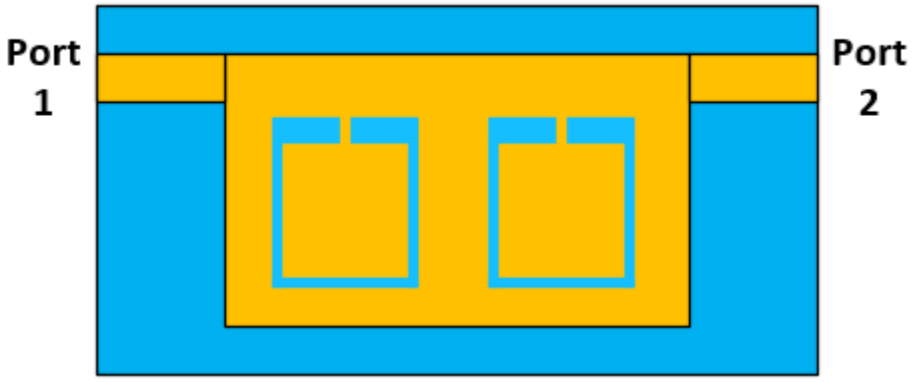

Figure 10. Procedure of the microfluidic channel mold filled with PDMS solution.

However, when the metallic liquid was inserted into the channel, the operating frequency varied from 2.205 to 2.56 GHz with practically little change in the coupling coefficient. For the fractional bandwidth, there was an improvement of about 2.58% compared to when the channel was empty. This is retributed to the structure of the CSRR varies and the reduction in the outer Q factor. For quick verification, the measurement was repeated when the liquid was completely removed from the channel, and the measured results are quite like those recorded before the liquid metal was injected. A switchable liquid metal alloy bandpass/bandstop filter was presented in the work of [31], in which there is no need for biasing. EGaIn with PDMS is used as a liquid metal on a Roger RT/Duroid 5880 substrate. A third-order balanced reconfigurable bandpass microstrip filter operating in seven different bands was proposed in [35]. Sodium hydroxide (NAOH) is used as a liquid metal on a substrate Roger RT/Duroid 5880. Figure 11 presents the prototype of the microstrip filter with the microfluidic channel.

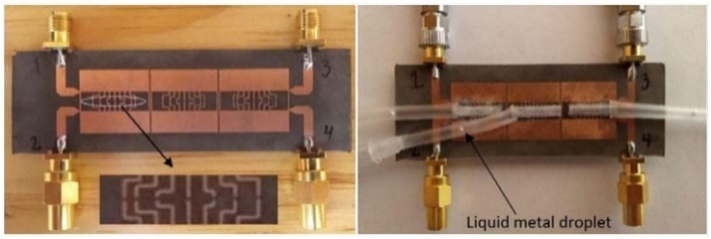

(**a**) (**b**)

Figure 11. (**a**) Fabricated design of the microstrip filter; (**b**) mircrofluiding channel implementation [35].

Another research was implemented on tunable microstrip filters [36]. At 10 GHz, the resonators are developed on a Rogers RT/Duroid 5880 substrate with a thickness of 0.254 mm. The basic concept is to use a suspended substrate with an integrated network of plastic tubes that can be filled selectively with a high-permittivity dielectric fluid, such as water. The electrical length of certain elements of MS circuits may be changed in a controlled and reversible manner by changing the substrate's effective permittivity in this way. Tunable stub resonators based on suspended and inverted MS lines are constructed and characterized in frequency and temporal domains as proof-of-concept. The same concept is then used to create a fourth-order bandpass filter with a fractional bandwidth of 40% that operates at 5 GHz. An adjustable range of 19.5% is demonstrated, with an insertion loss of 0.6 dB.

Enrique Gonzalez-Carvajal et al. presented an mm-wave tunable microfluidic reconfiguration bandpass filter in [37]. This BP filter was found attractive for wideband tunability, low loss, and high power-handling capacity. Different layers of fluids such as fused silica, parylene, and FC-40 were used in a microfluidic channel. Roger RO4003C was chosen for selectively metalized plates (SMP). Figure 12 shows the prototype of the bandpass microstrip filter with microfluidic channel details. The comparison about parameters about different microfluidic reconfigurable filters is given in Table 2.

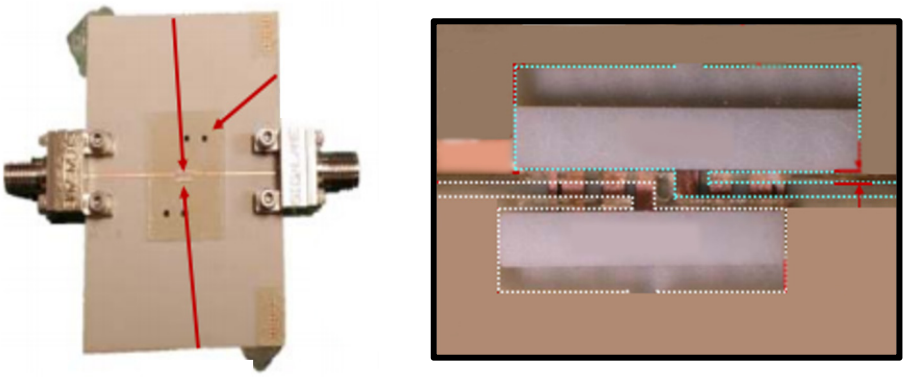

(**a**) (**b**)

Figure 12. (**a**) Prototype of BPF; (**b**) mircrofluiding channel details.

Table 2. Comparison analysis of microfluidic reconfigurable filters.

Reference	Fluidic Material/Substrate	Frequency (GHz)	Technique/Filter Type	Applications	Advantage	Disadvantage
[27]	3 M FC-40/Rogers 6010.2 and PDMS	4 to 1.5 GHz	microstrip line comb-line filters	4th-order filter	Reconfigurability/high tunable-frequency range/IL = 3 dB and RL = 9.5 dB, power-handling capacity = 15 W	Susceptible to environment change and EM radiation
[28]	Eutectic gallium indium liquid metal mixed up with sodium hydroxide/Rogers UL2000	1, 1.4, and 1.8 GHz	Metal liquid switches and dual-mode ring resonators	RF filters	Reconfigurability/ IL = 0.47–0.68 dB	Need of biasing/temperature sensitive
[29]	eutectic gallium indium (EGaIn)/Roger Duroid 5880	Lower band = 1.85 GHz, Higher band = 3.06–2.95 GHz	Split-ring resonator	Dual-band bandpass filter	Fluidically tunable/dual mode/ IL $\leq$ 2.72 and $<$ 3.21	Need of biasing/temperature sensitive
[30]	Zoflex conductor/PDMS	6 GHz	Planar microstrip circuit	3 dB-branchline coupler	Bandwidth is wider than single conventional coupler/RL and isolation >18 dB, IL > 4 dB	Need of biasing/temperature sensitive
[31]	Eutectic gallium indium (EGaIn)/Roger 5880 and PDMS	2.205 to 2.56 GHz	CSRR/QMSIW	Bandpass filter	Switchable frequency/ RL > 15 dB, IL < 1.5 dB	Need of biasing/temperature sensitive
[32]	Distilled water	C band	SIW	Fluidic tuning of microwave oscillators	Frequency tuning/tuned over a 110 MHz band	Need of biasing/temperature sensitive
[33]	Eutectic gallium indium (EGaIn)/thermoplastic acrylonitrile butadiene styrene	K band	Using multiline technique	Microfluidically controlled waveguide switch	Low cost, lightweight, RL > 15 dB IL = 0.5 dB	Temperature sensitive
[35]	Sodium hydroxide (NAOH)/Roger RT 5880	S band	Microstrip	3rd-order bandpass filter	Reconfigurability/ RL < 40 dB IL = 1.67–2.17 dB	Temperature sensitive
[37]	(fused silica, perylene, and FC-400)/Roger RO4003C	28 Gto 41 GHz	Microstrip	Tunable mm-wave bandpass filter	Reconfigurability/low loss/high power-handling capacity IL = 1.9–3.1 dB	Need of biasing/temperature sensitive

4. Fluidic Antennas

Fluidics is very common in antenna technology, especially for feeding networks [38–40]. Abhishek Dey et al. presented a microfluidically switched broadband tunable metallic liquid monopole antenna [38]. The design is based on the volume of the movable metallic liquid where the micropump unit is coupled using a microstrip feedline capacitively. To enhance the capacitive coupling at the feeding point, a microfluidic channel model is developed by bonding between 0.0254 mm-thick liquid crystal polymer and PDMS substrates. The design was measured for frequency band 1.29 to 5.17 GHz, and this monopolar antenna can also be operated as a component to make a broadband frequency tunable with peak gain antenna aperture without any further microstrip unit. The schematic of this presented antenna is shown in Figure 13.

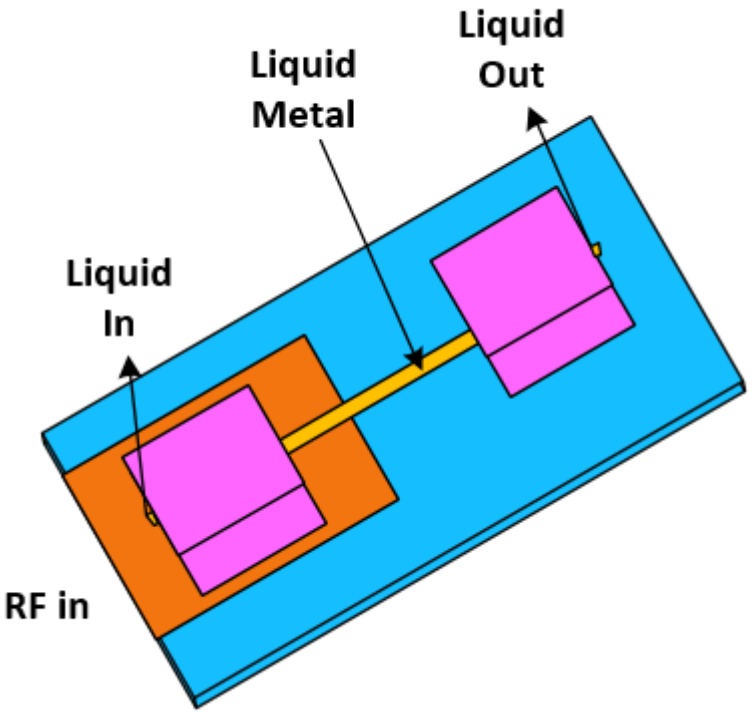

Figure 13. Liquid metal monopole.

Using deionized water R.R. Franklin and C. Murray were structured an independently tunable slot antenna operating frequencies water [40]. Two resonating frequency channels are introduced. The resonating bandwidth of the first channel is 3.3 GHz to 4.2 GHz, and the second channel is 5.2 to 8 GHz. A ringed slot antenna with a cohesive surface fluidic channel is carefully designed and investigated to obtain independent control on these two channels. The schematic of the final design is presented in Figure 14a. The electric field distribution using the simulator for both channels is discussed in Figure 14b,c.

In concluding remarks, high dielectric loss fluid is suitable for channel control but caused to degradation the peak gain and using lower dielectric constant fluid gain degradation is reduced. In the work of [41], to nullify the effect of a human hand on antenna performance, a microfluid-based planar inverted F antenna impedance tuning is introduced. The impedance matching is attained by changing the impedance of the liquid metal alloy stub injected by the piezoelectric micropump. The antenna was printed on FR-4 substrate and worked at 900 MHz. The injection and extraction of microfluidics are faster and easier in this design as compared to the work of [42,43], where liquid metal is constantly inserted into a long fluidic channel. The microfluid channel was fabricated inside the PDMS (polydimethylsiloxane). The oxidation problem is solved by pre-treating the microfluid channel with Nafion solution. The fabricated model of the antenna with a microcontroller is presented in Figure 15.

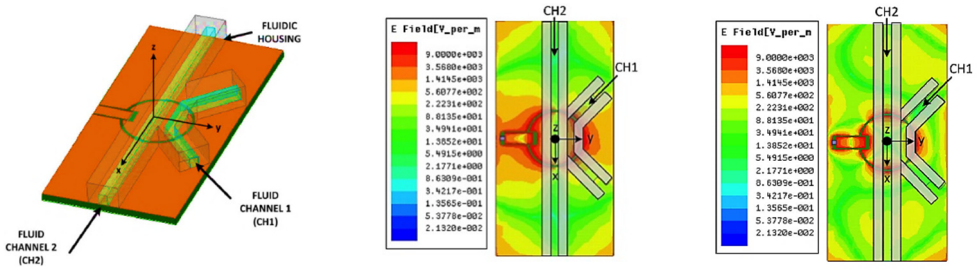

(**a**) (**b**) (**c**)

Figure 14. (**a**) The schematic of proposed antenna structure; (**b**) the E-field distribution for first resonating mode (4.2 GHz); (**c**) the E-field distribution for the second resonating mode (8.07 GHz) [40].

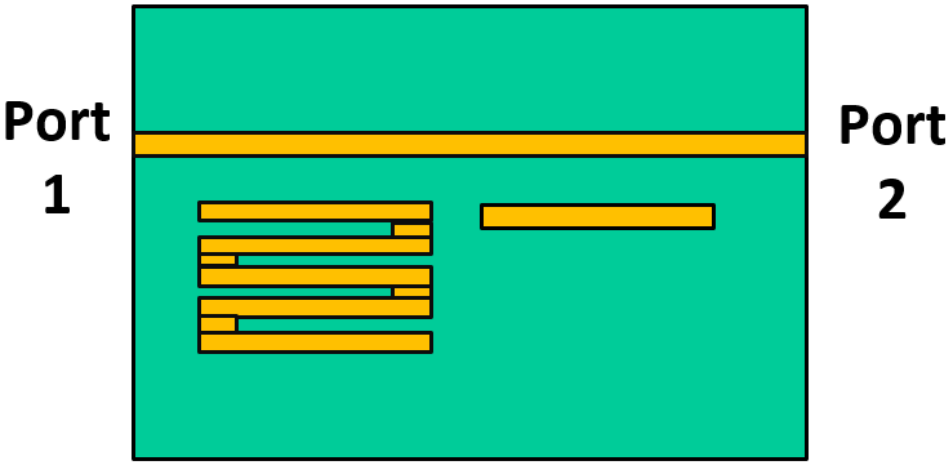

Figure 15. Photograph of the Microfluidic impedance tuner.

A reconfigurable double stub tuner with Galinston liquid metal is proposed in the work of [44]. The whole structure is supported on Roger RT/Duroid 5870 substrate. The input impedance can go beyond 75 ohms when the resolution in the liquid metal pumping is increased. Three-dimensionally printed multiple polarization switchable E-shaped microfluidic antenna was introduced in [45]. This is a dual-polarized microfluidic patch antenna, i.e., linearly polarized and circularly polarized fabricated on Roger RT5880. Multilayer prototype microfluidic E-shaped patch antenna is presented in Figure 16.

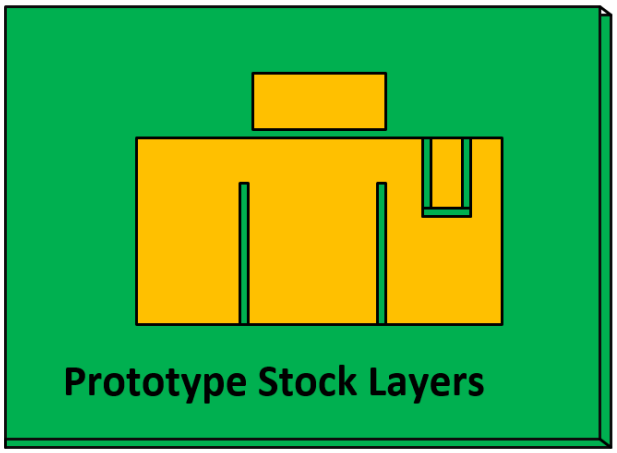

Figure 16. Multilayer prototype microfluidic E-shaped patch antenna.

On the other hand, a wideband switchable slotted patch antenna based on microfluidic was introduced in [46]. The patch antenna was printed on the Roger substrate RT/Duroid 5880. The fabricated model of the switchable slotted patch antenna is presented in Figure 17.

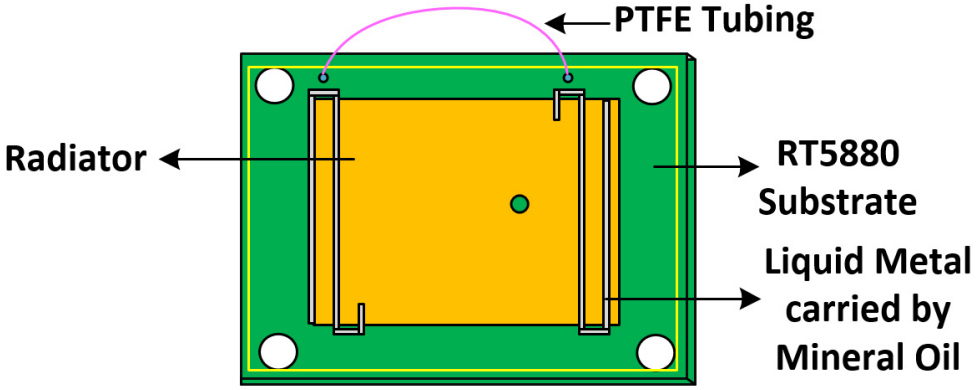

Figure 17. The picture of the microfluidic structure.

Kai Kit Wong et al. presented a fluidic flexible antenna that can switch its position easily in vacuum [47]. Within a small space, the antenna can attain the capacity of the multiple antenna maximum ratio combining (MRC) system. A low-cost novel monopolar closed-loop fluidic antenna system that can switch itself in real-time. An Agilent 85070E probe kit is used to measure the loss tangents and the dielectric constants of the poly-dimethylsiloxane (PDMS). Two kinds of ionized solutions, NaCl and KCl, were used as fluidic materials. The whole system was fabricated on FR-4 (ε_r = 4.3, tan δ = 0.008) substrate. The antenna system covers the frequency range from 3.2 to 5 GHz. Isometric view of the 3D-printed monopolar fluidic antenna and simulated h-field at 3.5 GHz as presented in Figure 18.

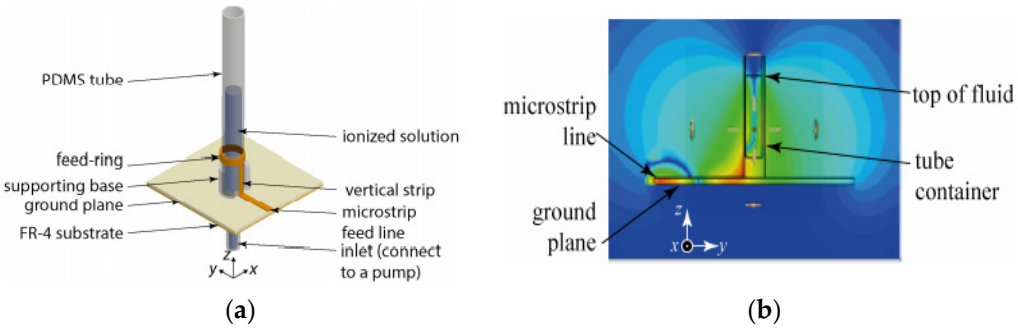

Figure 18. (**a**) Isometric sight of the 3D-printed monopolar fluidic antenna; (**b**) simulated H-field at 3.5 GHz [47].

A miniaturized monopolar water patch antenna using ethyl acetate substrate was presented in the work of [48]. This water patch antenna is an elective applicant of a crystalline antenna.

It involves three layers: first layer of water patch, second layer of ethyl acetate substrate, and the third layer of water ground plane. The proposed water patch antenna is shown in Figure 19. The overall summary about different fluidic antennas is given in Table 3.

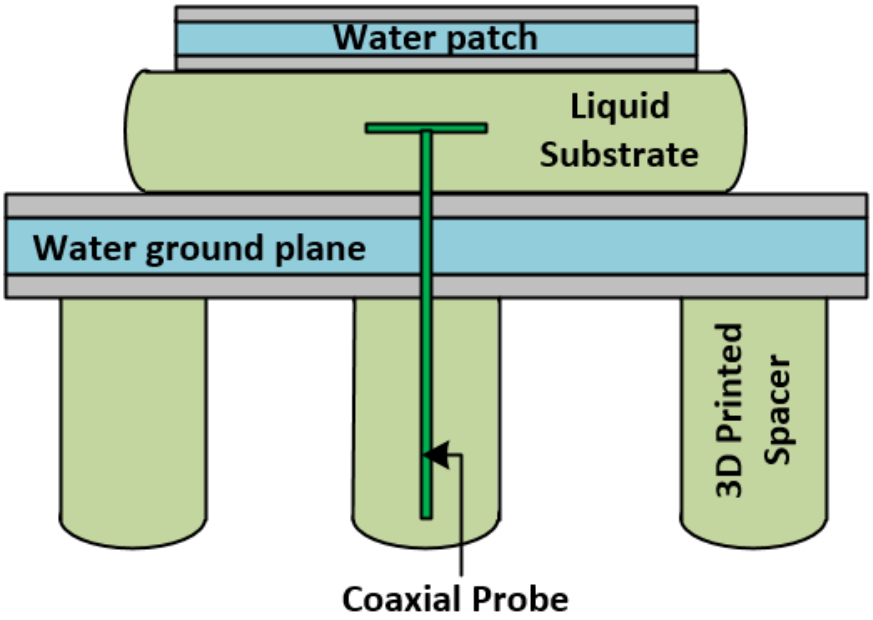

Figure 19. Miniaturized monopolar water patch antenna.

Table 3. Comparison analysis of fluidic antennas.

References	Fluidic Material/Substrate	Bands	Techniques/Antenna Type	Applications	Advantages	Disadvantages
[38]	EGaIn/PDMS/Roger RT Duroid 5880	2.5 GHz	Liquid metal alloy as fluidic switch	Switchable bandpass/bandstop filter	Low cost, no need of biasing, high temperature sensitivity, RL > 15 dB, IL = 0.5 dB	-
[39]	Low-loss Teflon/(PDMS + liquid crystal polymer + Roger 5880)	1.29 to 5.17 GHz	Microfluidical reconfiguration	Micropump driving circuit, microcontroller	Miniaturized, tuneable array	Susceptible to certain applications that require compact size
[40]	(Air + acetone + DI water)/FR-4	3.3–4.2 GHz for 1st band, 5.2–8 GHz for 2nd band	Surface-integrated fluidic channel	Channel placement locations	-	Susceptible to environmental change
[42]	PDMS/Rogers RT/Duroid 5880	900 MHz	PIFA	Piezo electric-micropump	Perfect impedance matching	Susceptible to the environment
[43]	PTFE, polyimide, Galinstan, Rogers RT/Duroid 5880/	3.37 to 6.02 GHz	Continuous electrowetting (CEW)/liquid metal slugs	Frequency-tuneable amplifier	The amplifier can be tuned with higher precision	-
[44]	Polystyrene/Roger RT/DUROID 5870	3.275 GHz	Liquid metal reconfigurable double stub tuner	Automated pumping and tuning mechanism	High tuning resolution	With high resolution, input impedance beyond 75 points
[45]	PTFE, RT5880 PCB	2.4 GHz	3D-printed microstrip	Tuning and switching mechanisms	Multiploidizations, highly effective, reconfigurability	-
[46]	Optical clear acrylic (Veroclear)/Rogers RT/Duroid 5880/	2–2.5 GHz	Microstrip slotted patch antenna	3D printing	Wideband/switchable/high resolution/reusable	More transition time
[47]	(NaCl + KCl)/FR-4	3.2 to 5 GHz	Closed-loop system/microstrip feedline	Multiple communications/3D-printed fluidic antenna	Low loss, low cost, reconfigurable, efficient,	Not flexible
[48]	Water patch antenna/ethyl acetate	1.9 GHz	Monopolar patch with high-permittivity substrate	Optically transparent	Low cost, miniaturized, transparent, ease of access, flexible	Less efficient

5. Fluidic-Based SPST Switch

Microfluidic is also very useful in controlling the switches of RF and microwave devices. Switches such as single pole single through switch (SPST) and single pole double through switch (SPDT) are some of the popular RF and microwave switches available. The SMPs-based high power-handling and wider bandwidth line combining filter were proposed using capacitive loading and length variation concept. According to some recent research, up to 10 m microfluidic channel walls were proposed in [49] with a high-speed feeding switch for millimeter-wave beam-steering focal plane arrays. Although the liquid metals switching has limitations due to oxidization and low conductivity, these problems were solved using selectively metalized plates (SMPs). Reference [50] reports that recently some researchers were designed a combined actuation of the microfluidic switchable millimeter-wave SPST switches. It exhibited a low insertion loss (IL) of about 0.42 dB, wide bandwidth, and fast switching. The combined piezoelectric reconfiguration and the actuation time of the design is 1.12 ms with a working bandwidth from 22 to 40 GHz. The piezoelectric actuation is based on the method discussed in [48]. Where frequency tunability is attained by employing a portable metalized plate in the microfluidic channel. The design is coupled capacitively with a microstripline through 12 µm-thick non-conductive benzo cyclobutene (BCB), used to make a bond, and wrapped the polydimethylsiloxane (PDMS). The comparison between fluidic-based SPST switches is given in Table 4.

Normally, the water droplet has a capacitive contact with a dielectric, as reported in [51]. Chen et al. described the design of a new wideband microfluid-based reflective and absorptive switch [52]. This water-based switch works more than 20 GHz. They are cheaper than liquid metal switches. The major issues discussed in this design are less isolation and droplet evaporation because of substrate losses. Droplet is modeled in a packed form in this design, and the isolation is practically improved, and more than 15 dB for whole operating bandwidth is successfully attained. Conventional droplet size measurement technology discussed in [52] was used for the capacitive switch. In this work, it is studied that if the number of droplets in a coplanar waveguide (CPW) is increased to a droplet 2 to 3, the isolation also increases from 15 to 20 dB, respectively, at 20 GHz. From the first absorptive switch, only a partial E-field is enclosed by the water droplet while, for the next absorptive switch in Figure 20, the water surrounds the CPW line, producing an E-field to circulate through its volume.

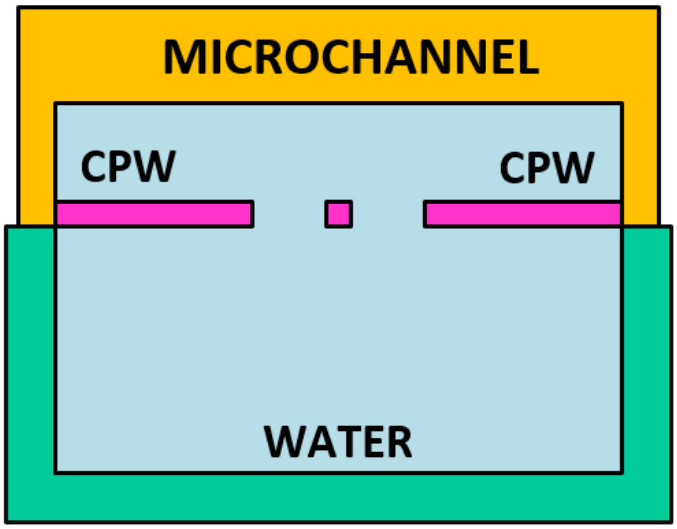

Figure 20. 2nd absorptive switch in which water surrounds the CPW line.

The applications of RF (radio frequency) MEMS (micro electro-mechanical systems) switches in space hardware need extensive study and test efforts. An electrowetting concept of the liquid metal droplet is proposed in [53]. A silicon-based MEMS technology SPDT

RF switch was reported in [54]. Moreover, in [55], a low actuation power employing a liquid metal-based fluid is designed by means of continuous electrowetting and air bubbles trapped. It has a wide bandwidth and a low-loss shunt switch. With this low actuation power, the bandwidth of the structure ranges from 4 to 16 GHz with a 10 dB isolation, and less than 5 dB insertion loss is successfully achieved. The OFF and ON working states of the device were performed satisfactorily by injecting an air bubble and liquid metal into the capillary.

A reconfigurable slot array antenna with a radiofrequency MEMS switch for X-band applications was proposed in [56]. External micropumps and slow speed are the major drawbacks in microfluidic antennas. To overcome these issues, microfluidic switches for millimeter-wave beam-steering antenna arrays were presented in [57]. The microfluid channel is occupied by low-loss liquid FC-40. Four elements antenna array is operated with an insertion loss of <0.9 dB and isolation of <18 dB at 18 GHz. The fabricated model of the antenna with a microcontroller.

Table 4. Comparison analysis of fluidic based spst switches.

References	Fluid/Substrate	Band	Technique/Antenna Type	Applications	Advantages	Disadvantages
[49]	Roger RO4003C	Ka-band	Microfluidic reconfigurable	Piezoelectric micropump actuation	Closed loop, reconfigurability, position sensing IL < 0.2 dB	Toxic for the environment
[50]	(SU-82075 Microchem + parylene)/ Roger RO4003C	22 to 40 GHz	Microfluidic microstrip	SPST reconfigurable switch	Low loss, wideband, high reliability, low reconfiguration time, superior power-handling capacity/ IL = 0.42 dB, isolation > 20	SPST switch performance is not so good, not closed loop
[51]	FC-40, benzocu-clobutane (BCB)/PDMS, RO4003C	1.7–3.5 GHz	Microfluidically tunable monopole antenna	Piezoelectric micropumps-based SPST switch	High RF power, highly efficient, tunable	Not closed loop
[52]	Teflon/galinstan solution/PDMS	20–100 GHz	Coplanar waveguide technique	MEMS switch	Very wideband, nontoxic for the environment, IL < 1.3 dB Isolation > 20 dB	-
[55]	PTFE, polyimide, polystyrene	4–16 GHz	Coplanar waveguide technique	Shunt switch	Low power, wideband, IL < 5 dB, Is > 10 dB	Toxic for the environment
[57]	Low-loss liquid FC-40/RO4003C	30 GHz	Four elements millimeter-wave beam-steering antenna array	Microfluidic switches	Less actuation time, low loss, high power-handling capacity/IL < 0.9 dB, isolation < 18 dB	
[58]	FC-40/RO4003C	28GHz	Microfluidically reconfigurable spatially adaptive antenna array (MRSA)	Millimeter-wave wireless channel control systems	High gain, reconfigurability, long microfluidic channel,	Slightly misalignment in fabrication

Microfluidic-based reconfigurations of a spatially adaptive antenna array (MRSA) for millimeter-wave wireless channel control systems were proposed in [58]. The microfluid channel is occupied by low loss liquid FC-40 on a Roger RO4003C substrate and the sidewalls of the channel executed from Photo-resist SU-8. The fabricated model of the MRSA is shown in Figure 21.

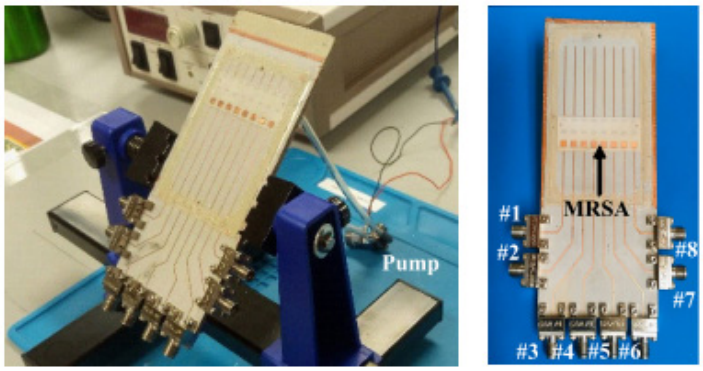

Figure 21. Fabricated model of the MRSA [58].

6. Microfluidic Sensors

A gas sensor contains an active layer and a transducer. It has many applications, which include home control, industrial safety, environmental monitoring and control, quality control of agricultural food products, biomedical diagnostics, etc. [59]. Different technologies that involve various transduction principles are used for gas sensing. This includes electrochemical, conductometric optical, acoustic wave, plasmonic transduction, impedance spectroscopy, and microwave. The need for having real online monitoring in remote sensing applications that have been deployed wirelessly has recently made microwave-based gas sensing popular. Microwave is one of the frequency bands in the electromagnetic spectrum that has been used for remote sensing applications. The performance of surface-micromachined devices may be superior to that of bulk-micromachined devices, according to research. At 1 mW heater dissipation, the sensitivity for hydrogen in the air was determined to be 60 V per percent H_2. As stated in the section, sensitivity, reaction time, selectivity, compact size, and low power consumption are all aspects that influence the performance of any sensor. According to multiple studies on various gas sensors, the current trend is to build gas sensors employing microelectronics technology, which offers the advantages of compactness and low power consumption. The microwave transduction principle is created on the response of the dielectric sensing material, which has propagative structures when exposed to the target gas [60,61]. Finally, RF sputtering from the Pt target (99.999%) via a tape mask at an RF power of 142 W and a sputtering pressure of 7 mTorr was used to coat a Pt film as a catalyst over the ZnO layer. However, different types of sensing materials have also been deployed as sensing layers such as metal oxides [62], conducting polymers [63], organic nanomaterials [64], etc. In [62], a C_2H_2/H_2 (20/80 sccm) gas combination was used to create the plasma in the RF-PECVD growth reactor. The process parameters for growing CNTs were set to 100 W, 1.5 Torr, and 450 °C, respectively, for rf power (13.56 MHz), working pressure, and temperature. The most used gas sensors are the conductometric sensors that use oxides as an active layer and require high operating temperature and high-power consumption, and this makes them costly. Therefore, there is the need for having gas sensors that are passive, wireless, cost-effective, and can operate at room temperature. This makes microwave-based gas sensors a suitable candidate to achieve these characteristics. The major benefits of these sensors comprise low power consumption, small size, low cost, wireless operations, and real-time online monitoring. Microwave gas sensors have been used for gas detection, humidity sensing, flow sensing, and liquid sensing, and microfluidic systems [61].

Conducting polymers are promising sensitive materials due to their numerous advantages, which include low cost, high sensitivity, and low temperature. Poly (3,4-ethylene dioxythiophene) polystyrene sulfonate (PEDOT. PSS) have been used as sensing material for humidity sensing due to their outstanding properties. An actual humidity sensor was created on a microwave resonator attached with PEDOT. PSS polymer layer has been presented by [65]. To increase the sensitivity of the sensor, the polymer layer is placed inside

the area that has been the powerful E-field in the resonator. It was fabricated on a PCB, which was excited by electric and magnetic field coupling. The results obtained showed that the transmission coefficient (S21) and operating frequency vary with comparative humidity varied from 5% to 80%. Fabricated humidity sensor, S_{21} frequency response of DSRR, and S_{21} isotherm characteristics of the sensor were obtained as illustrated in Figure 22.

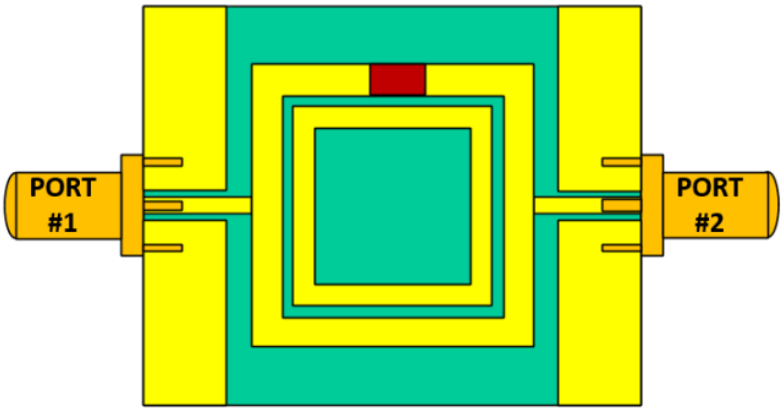

Figure 22. Picture of the Fabricated humidity sensor.

In the same way, it has been presented by [66] that a resonator fixed within a 3D-printed fluidic channel might be used for fluid sensing implementations. The sensor was fabricated to operate among 5.3–5.8 GHz operating bands with a Q factor of 116 and a resonating amplitude of −15 dB. The sensor was placed inside the microfluidic channel to enhance the sensitivity and accuracy of the sensor. The input transmission line was printed on a flexible Rogers substrate RT5880, whereas Rogers Ultralam 3850 was used for the ring structure with copper as the material for striplines, input lines, and resonators using the 3D printing process. HFSS simulations were used to validate the improvement of the Q factor and the resonating amplitude by changing the values of the resonator comparative to the feedlines. Transmission parameters (S_{21}) obtained from the vector network analyzer showed different variations in the shift in resonant frequencies for different liquids, including water, methanol, isopropyl alcohol, and reverse osmosis water. Water, which has the highest relative permittivity, showed the largest resonant frequency shift of about 500 MHz. The minimum detectable limit was found to be 0.1% ethanol experimentally. However, there was a suitable agreement between simulation and measured results.

Sensitivity and high accuracy are key performance parameters for an ideal sensor. This could be enhanced using open-loop resonators, split-ring resonators, and metamaterials. Split-ring resonators have also been used to enhance the sensitivity in microwave-based sensors. As shown by the work of [67], a planar microstrip ring resonator structure was developed on an alumina substrate, as illustrated in Figure 23. A simulation was accomplished using finite element modeling (FEM) software in COMSOL. The microwave sensor was designed to operate at 8.5 GHz at room temperature with Fe-zeolite as the sensing layer film. The change in resonant frequency and S11 was recorded as the sensor response when exposed to the target gas. The sensor was revealed to various concentrations of ammonia varying from 0 to 500 ppm and then from 500 to 1000 ppm, and the change in resonant frequency was recorded for each ammonia gas concentration.

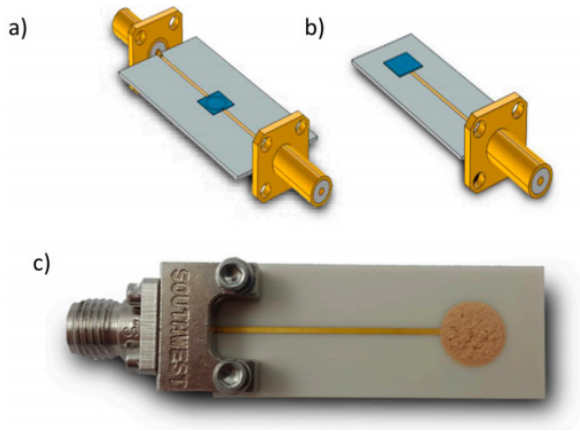

Figure 23. Three-dimensional sensor models with gas-sensitive cover layers; (**a**) types of transmission; (**b**) reflection resonator type; (**c**) fabricated microwave ring transducer [67].

The same sensor was also tested as a humidity sensor for water adsorption. Similarly, an OCSRR was used for microwave-based gas sensors [68]. The sensor was constructed on a couple of similar unpaired lines, each loaded with OCSRR, and was arranged for the estimation of solute absorption in fluidic solutions and used for the evaluation of complex dielectric constants in fluids (see Figure 24).

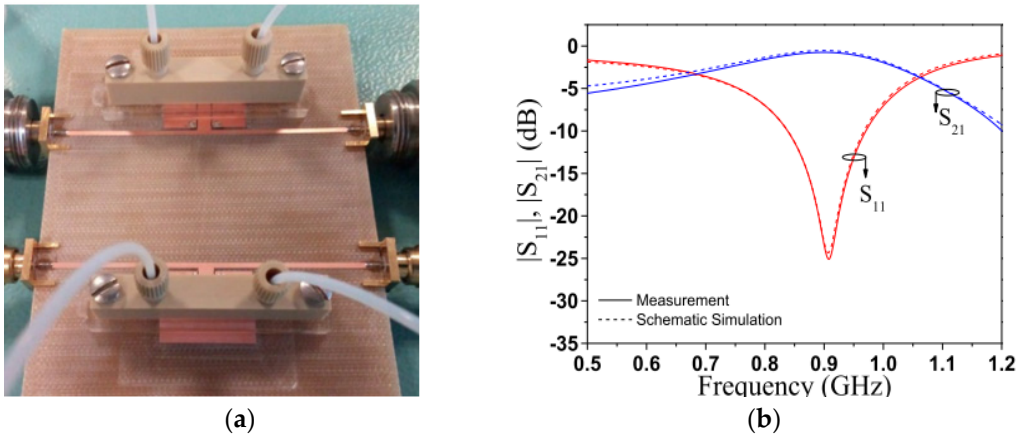

(**a**) (**b**)

Figure 24. (**a**) Prototype sensor containing connectors and the fluidic channels; (**b**) reflection coefficient of the single OCSRR loaded with DI waster [68].

In another research by [69], a microstrip gas sensor that was based on a trapezoidal spiral resonator was presented. The resonator was covered by titanium oxide nanoparticles as the sensing layer. The reflection and transmission coefficients were obtained before and after coating of the sensing layer, and the shift in resonance frequencies was obtained. The measurements were carried out between 1 and 8 GHz, and multiple resonances were observed. Different ammonia concentrations from 50 to 300 ppm were tested for the sensor. Results obtained presented a decent response to NH_3 gas with a response time that was lower than a minute. The sensor exhibited suitable reversibility and stability with a mono-frequential temporal analysis. Maximum feedback was observed at 7.76 GHz with a return loss of 0.45 dB at 300 ppm ammonia gas.

A parallel plate capacitor could also be used to improve the stored electrical energy in the sensitive area that is discovered during measurements, as shown by [70]. A resonator that is based on complementary electric LC was used for the sensor design. The sensor was simulated using HFSS and printed on a flexible substrate R04350 using PCB technology with a resonance frequency of 4.434 GHz. The sensor was employed to sense variations in a dielectric slab that was implanted into the gap of the channel. The fabricated sensor

was verified for the observation of the variations in the concentration of chloroform with permittivity of 4.81 and cyclohexane with permittivity of 2.02. The sensor detected a concentration of 5% and presented an improved performance of 304% as related to the sensor without the added top capacitance.

To enhance the sensitivity of planar microwave sensors, metamaterial-inspired resonators have been employed. This was shown by the work of [71], in which a novel metamaterial that has negative refractive index transmission lines was employed. The sensor was designed to operate at 2.5 GHz. MTM/MS and MS/MS sensors were simulated using HFSS and then fabricated on Rogers 5880 substrate. Different concentrations of ethanol and methanol ranging from 50 to 700 ppm were tested for both sensors. It was observed that the metamaterial-based sensor could sense liquid concentrations as less as 50 ppm relative to the conventional sensor, as shown in Figure 25. Results obtained showed a suitable correlation between analytical, simulation, and measurement.

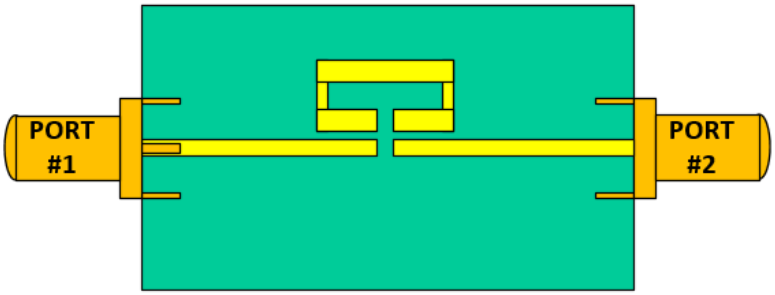

Figure 25. Metamaterial-based conventional sensor.

SAW-based resonators have also been used for gas-sensing applications. It was presented by [72] that dual SAW resonators with operating bands of 433.42 and 433.92 were used to design a dual SAW resonating system. The system was fabricated using PCB technology on FR4 substrate. The sensing layer was incorporated into the circuit as a standalone that is connected in parallel to the matching circuit. It consists of functionalized multiple walled carbon nanotubes and a poly-aniline layer. It was then tested toward various concentrations of hydrogen ranging from 1% to 2%. The sensor response was obtained based on the shift in resonance frequency. Results obtained presented an excellent response to H_2 gas and recovery times. The sensitivity of the sensor was found to be 3.2 Hz/ppm. Stub resonators have also been shown to have promising results in microwave gas sensing, as shown in the work of [73]. Fabricated flexible gas sensor and scattering parameters are presented in Figure 26.

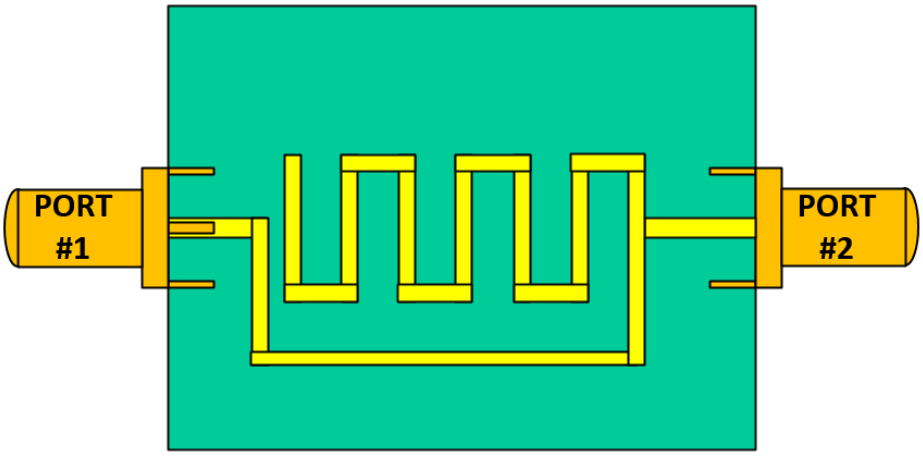

Figure 26. Photograph of the flexible gas sensor on Kapton substrate.

Similarly, capacitive resonators have also been used for the detection of environmental pollutants such as volatile organic compounds. This was shown by [74], in which two capacitive resonators were used for ethanol vapor detection. One of the resonators has the sensing layer, while the other was used as a reference. The sensing layer was made up of 3,4-ethylene dioxythiophene polystyrene sulfonate with multiwalled carbon nanotubes of ANSYS-HFSS was used as the simulation software using paper as the substrate, silver nanoparticles as the metal electrodes with PEDOT. PSS-MWCNTs as the sensing layer. The sensor was printed on flexible paper using inkjet printing technology. The sensor was then tested toward ethanol vapor of concentrations between 0 and 2000 ppm. The shift in resonance frequency was observed using the vector network analyzer (VNA) operating at 2 and 4 GHz. The sensitivity of the sensor was reported as −2.48 kHz/ppm, which is capable of gas sensing. A new device was placed on the test cell basement as shown in Figure 27.

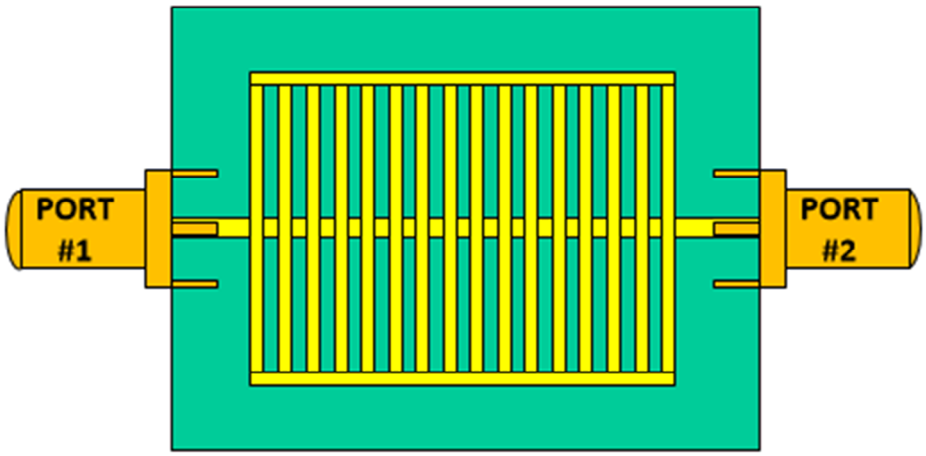

Figure 27. The picture of the device on paper placed on the test cell basement.

Carbon nanomaterials, including carbon nanotubes and grapheme have been used extensively in microwave sensors as sensing materials [60]. However, to enhance its sensitivity, metal loading on these materials further enhances its sensitivity as shown by (gas sensing by microwave transduction: review of progress and challenges Li Fangxin et al.) in order to enhance its sensitivity by using Pt loaded to detect small concentrations of hydrogen as low as 1 ppm. The large surface area of grapheme and the metal decoration proved enhanced sensitivity. In another research by [75], SIW cavity resonators for gas-sensing application have been reported in Figure 28. Both SRR and CSRR were printed and then covered with graphene grownup by CVD (chemical vapor deposition), and a layer of PMMA (polymethyl methacrylate) was blended on its peak. Operating bands shifts were noticed as 59 MHz for SRR and 157 MHz for CSRR when the sensor was kept in front of NH_3 gas.

In another study, a GHz frequency range passive voltage transformer using a mechanically tunable strip-line resonator at 1–2 GHz is proposed in the work of [76]. The stated sensor can detect low radiofrequency signals that may be used to wake up a sensor node in case there is a need to sense or send the information. At high radiofrequency frequency bands, the transformer is harder to implement owing to the low impedance of load capacitive loads. The transformer exhibited a 19.5 dB gain at 1.007 GHz and achieved gains over 19 dB with load capacitances of 0.8–2.4 pF. A piezoelectric AlN GHz transducer was also used to measure the gain of the resonator. An RF waveguide model has been developed, which matches experiments well for both frequency and gain responses. The schematic diagram of GHz resonator device is shown in Figure 29.

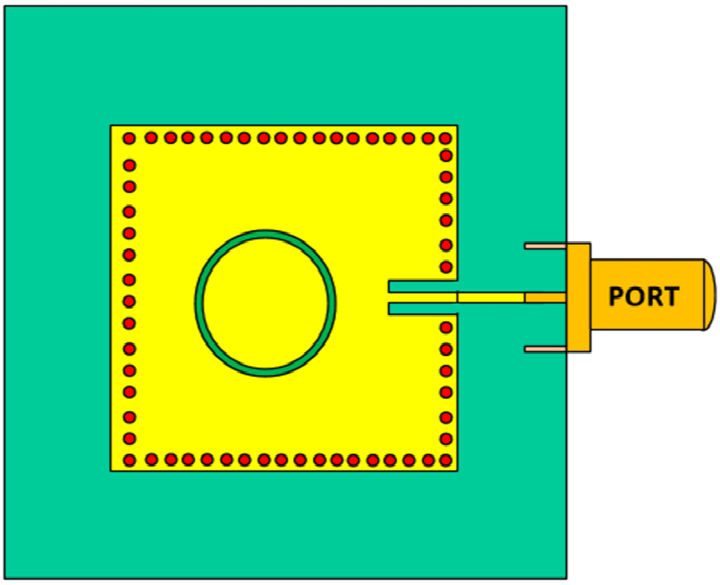

Figure 28. The picture of the SIW resonators.

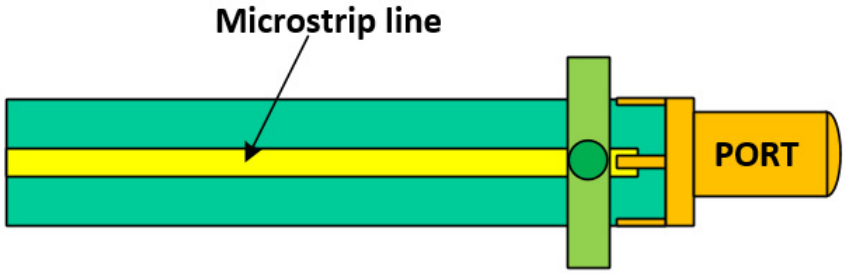

Figure 29. A schematic of the GHz resonator device.

For large-scale distant ethanol sensor applications, a unique flexible adjustable metasurface absorber is presented [77]. Periodic split-ring-cross resonators (SRCRs) and microfluidic channels made up the suggested metasurface absorber. The SRCR designs were created on paper using silver nanoparticle inks in an inkjet printer. On polydimethylsiloxane (PDMS) material, the microfluidic channels were laser-etched. For various liquids, the suggested absorber can detect changes in effective permittivity. As a result, by monitoring variations in resonant frequencies, the absorber may be employed as a distant chemical sensor. Full-wave modeling and measurement data are used to illustrate the performance of the proposed absorber. When the concentration of ethanol is raised from 0% to 100%, the resonant frequency increases from 8.9 to 10.04 GHz, according to the experimental data. Furthermore, the suggested absorber has exhibited a linear frequency shift from 20% to 80% of the varied ethanol concentrations.

In [78], the authors had reported the complementary split-ring resonator (CSRR)-based microfluidic chemical sensor. The major goal of this chemical sensor was to detect the presence of ethanol. On a Rogers RT/Duroid 5870 substrate, two tightly coupled concentric CSRRs loaded on a patch were first realized, and then a microfluidic channel was engraved on polydimethylsiloxane (PDMS) was integrated for ethanol chemical sensor applications. The structure's resonance frequency before loading the microfluidic channel was 4.72 GHz. When the ethanol content was changed from 0% to 100%, the dielectric perturbation phenomena caused a 550 MHz shift in the resonance frequency after loading the microfluidic channel. Various amounts of ethanol were tested and evaluated to determine the sensitivity range of the reported sensor. The measurement setup confirmed that our suggested sensor has suitable reproducibility and can detect 10% ethanol. The top view, CSSR's structure and overall view of the design is shown in Figure 30.

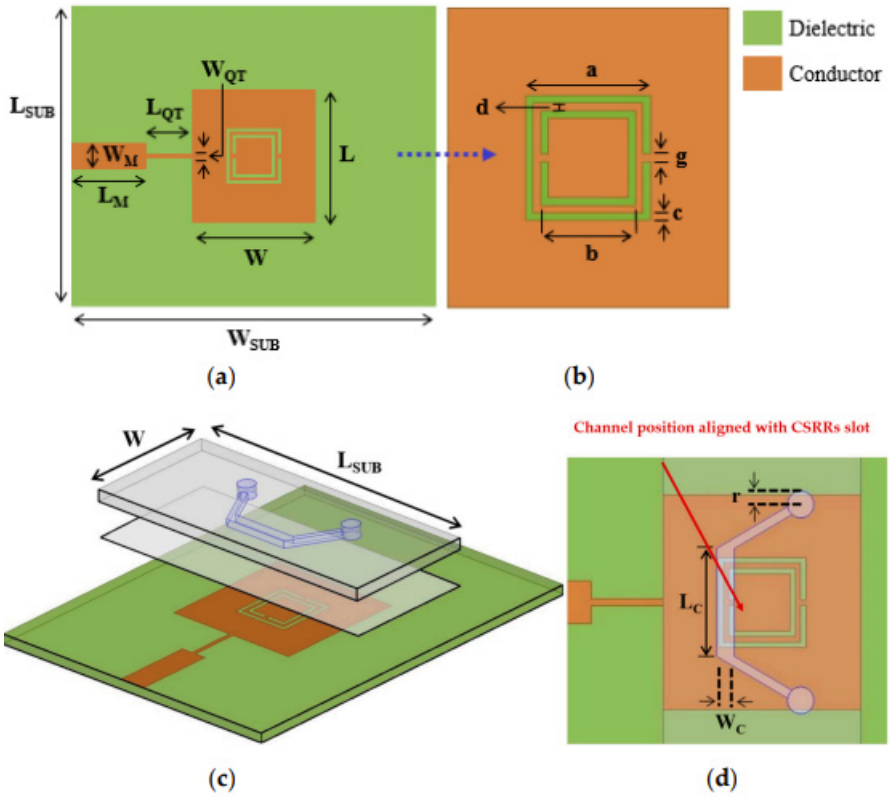

Figure 30. (**a**) Top view of CSRR-loaded patch fed by quarter-wave stub and microstrip line before loading PDMS; (**b**) zoom-in image of the CSRRs slot; (**c**) bird's-eye view of the proposed sensor with the microfluidic channel; (**d**) top view of channel alignment with CSRRs slot [78].

Gas-sensing devices are becoming increasingly used in a variety of settings, including interior spaces, industries, aircraft, and detectors for numerous harmful household gases and vapors [79]. Several distinct fluid/gas flows must be monitored for industrial applications since the flow of the fluid might affect the product under production. As a result, precise measurement is required to produce a high-quality product at the conclusion of the manufacturing process. Gas sensors are mostly employed in the petrochemical industry in the industrial world. Some carbon dioxide sensors, ammonia sensors, nitric oxide sensors, and other sensors can be used in specialized applications to detect carbon dioxide, ammonia, chlorine, and other dangerous gases [80]. The interaction between typical aroma composing components and the response of semiconducting gas sensors and one microgravimetric sensor is presented using some fundamental concepts [81]. The selection of sensor materials to manage baking and roasting operations has been based on several broad principles. Using a basic electronic nose with two to four oxide sensor components, important aroma molecules, such as 2-acetyl-1-pyrroline (typical pop-corn scent), were demonstrated to affect the toasting of white bread (no pre-selection by a chromatographic column necessary). Other uses, such as controlling meat roasting, will continue to be problems in the future. Sensor components that are sensitive to sup-ppm levels, as well as particular to key scent constituents, are needed. Finally, packaging, transportation, and aging of items during storage or usage can all affect flavor; some of these factors are covered in the work of [82]. Table 5 summarize the parameters comparison between different microfluidic sensors.

Table 5. Comparison analysis of microfluidic sensors.

References	Fluid/Substrate	Bands	Techniques	Applications	Advantages	Disadvantages
[61]	Polymer, carbon nanotube/ST X-CUT quartz substrate	157 MHz	Mass flow controller and photolithography	SAW gas sensor	Highly responsive to volatile gases, IL = 15 dB, attenuation = 9 dB	Only detect limited gases
[62]	ZnO nanoparticles/Pt catalyst	129.28 MHz for uncoated, 126.93 and 128.85 MHz for coated	Post-annealing process	SAW hydrogen sensor	Suitable repeatability and stability, largest frequency shift	Sensitivity may vary by temperature, material and area of SAW sensor
[63]	Carbon nanotube, ST-cut quartz substrate	433.93 and 915 MHz	Langmuir-Blodgett (LB)	Multiwalled SAW gas sensor	Low cost, highly gas sensitive	Sensitivity may vary by area of SAW sensor
[64]	Polyethyleneimine (PEI), ST-cut quartz substrate	69.4 MHz	Nanotubes	SAW nanocomposite-based sensors	Reduced noise level, better time response, highly gas sensitive	Sensitivity may vary by area of SAW sensor
[65]	Conducting polymer, polystyrene sulfonate/printed circuit board (PCB) substrate	2.45 GHz	Double slip ring resonators (DSRR)	Humidity sensor	Outstanding repeatable response	Sensitivity may vary by material and the area of the humidity sensor
[66]	Polymer/Rogers RT5880 and ULTRALUM 3850 substrates	5.3 and 5.8 GHz	3D-printing microfluidic channel	RFID and liquid detection	High accuracy, sensitivity, affordable, reusable, environment friendly	Minimum detectable concentration toward ethanol-water mixture
[67]	Fe-Zeolite, alumina/RO4003C substrate	8.5 GHz	Planar microstrip ring resonators	Humidity and ammonia sensing	miniaturized, high accuracy, sensitivity	Sensitivity may wary with material
[68]	PDMS, polyester/FR-4	0.9 GHz	Open complementary slip ring resonators (OCSRR) and cross mode insertion loss	Differential permittivity sensors	Very sensitive to asymmetric loadings, highly sensitive	Less sensitive to symmetric loadings
[69]	Ceramic-filled PTFE/ Roger RT6202 substrate	1–8 GHz	Microstrip spiral resonator	Microwave-based ammonia gas sensor	Suitable reversibility and sensitivity	Limited sensitivity
[70]	Water, chloroform/Roger 5870	2.5 and 2.65 GHz	Quarter ring microstrip	Dual-band microwave microfluidic sensor	Temperature variant, overall loss decreases by increasing temperature	Limited sensitivity
[71]	Roger 5880 substrate	2.5–2.6 GHz	Metamaterial	MTM-infused MW sensor	High gain, negligible loss of power, large invariant coupling level	Less sensitive to low permittivity materials
[72]	Platinum, zirconium, GaPO4 layers on PCB	433.42 to 433.92 MHz	Double SAW resonator system	Hydrogen gas sensor	Insensitive to vibrations and other external disturbance	Limited sensitivity
[73]	Polymer/Kapton flexible substrate	0–6 GHz	Inkjet printing	Low coat MW flexible gas sensor	Harmful gas detection, for IoT applications, low power consumption	Less sensitive
[74]	Carbon nanotube, carbon composite polymer, flexible paper substrate	1–6 GHz	Inkjet printing	IoT, inkjet-printed chemical gas sensor	Low cost, multiwall, highly effective surface area	Limited sensitivity
[75]	PCB RO4350B	4.2 GHz	SIW cavity resonators, CSRR	Microwave gas sensor, ammonia gas detection	Low cost, highly sensitive, environment monitory solutions	Sensitivity may wary with material

7. Conclusions

This article reviews different aspects of fluidic couplers, power dividers, phase shifters, microfluidic reconfigurable filters, fluidic antennas, and microfluidic sensors. Different techniques for fluidic couplers, power dividers, phase shifters are discussed in this review, including tunable branchline coupler [19], microstrip hybrid modified coupler [23], inverted microstrip line with loaded split-ring resonator (SRR) [20], low-cost instant inkjet printing [21], microfluidic [22], modified PI-shaped transmission lines (TL) [24], miniaturization [25], instant inkjet printing silver nano [26]. Microfluidic materials, which include 3 M FC-40 [27], EGaIn liquid metal [28] mixed up with NaOH [34], Zoflex conductor [30],

distilled water [32], thermoplastic acrylonitrile butadiene styrene, fused silica, and parylene, show long-period stability of electric properties when enclosed in microfluidic channels [38], printed on substrates such as Rogers 6010.2, PDMS, Rogers UL2000, Roger Duroid 5880, Roger RO4003C, etc. Microfluidic antennas possess extraordinary flexible properties as radioactive elements in antennas, where 90% total radiation efficiency was sustained for fluidic antennas irrespective of 50% applied strain.

Different technologies that involve various transduction principles are used for gas sensing. This includes electrochemical, conductometric optical, acoustic wave, plasmonic transduction, impedance spectroscopy, and microwave. The major benefits of these sensors contain low power consumption, small size, low cost, wireless operations, and real-time online monitoring. Microwave gas sensors have been used for gas detection, humidity sensing, flow sensing, and liquid sensing, and microfluidic systems [60]. Since the ideal sensors have properties defined by selectivity, sensitivity, fast recovery time, and high response time. Every sensor technology is progressing in order to achieve the optimum properties of an ideal gas sensor. The tendency is to construct the sensor to keep the size as compact as possible. The SAW has all these features of an ideal gas sensor. This is the technique that employs small size, less cost, and less power consumption devices for gas sensors. Carbon nanomaterials have been used extensively in all different types of sensors in order to enhance their sensitivity as a result of their large surface area. However, more research needs to be performed by using hybrid materials such as grapheme with polymer and other metal oxides. The use of metal-decorated materials should also be explored for improved sensitivity and selectivity. Research could also be performed in microwave sensors by also using novel nanomaterials. In terms of measurement, more research should be performed to measure the return loss as a measure of gas response and not only focus on frequency shifts alone. The use of nanomaterials as sensing layer advanced researchers must pay much attention to this useful property for gas sensors as it saves energy and power consumption.

Author Contributions: Conceptualization, S.A.B., K.N.P., S.A., S.K.A.R. and Z.Y.; methodology, S.A.B., S.A., A.G., K.N.P. and A.L.; software, S.A.B., S.A., A.G. and M.N.; validation, S.A.B., A.G., S.A., K.N.P. and A.L.; investigation, S.A., A.G., S.A.B., M.N., Z.Y. and A.L.; writing—original draft preparation, S.A. and A.G.; writing—review and editing, S.A.B., S.A., K.N.P. and Z.Y.; supervision, A.G.; funding acquisition, S.K.A.R., M.N. and A.L. All authors have read and agreed to the published version of the manuscript.

Funding: This research received no external funding.

Conflicts of Interest: The authors declare no conflict of interest.

References

1. Ahmad, S.; Paracha, K.N.; Sheikh, Y.N.; Ghaffar, A.; Butt, A.D.; Alibakhshikenari, M.; Soh, P.J.; Khan, S.; Falcone, F. A Metasurface-Based Single-Layered Compact AMC-Backed Dual-Band Antenna for Off-Body IoT Devices. *IEEE Access* **2021**, *9*, 159598–159615. [CrossRef]
2. Chan, K.Y.; Ramer, R.; Mansour, R.R.; Guo, Y.J. 60 GHz to E-Band Switchable Bandpass Filter. *IEEE Microw. Wirel. Compon. Lett.* **2014**, *24*, 545–547. [CrossRef]
3. Park, S.J.; Lee, K.Y.; Rebeiz, G.M. Low-Loss 5.15–5.70-GHz RF MEMS Switchable Filter for Wireless LAN Applications. *IEEE Trans. Microw. Theory Tech.* **2006**, *54*, 3931–3939. [CrossRef]
4. Chan, K.Y.; Fouladi, S.; Ramer, R.; Mansour, R.R. RF MEMS Switchable Interdigital Bandpass Filter. *IEEE Microw. Wirel. Compon. Lett.* **2012**, *22*, 44–46. [CrossRef]
5. Kodera, T.; Caloz, C. Multi-function reconfigurable microwave component based on a switchable FET circuit. In Proceedings of the 2013 IEEE MTT-S International Microwave Symposium Digest (MTT), Seattle, WA, USA, 2–7 June 2013.
6. Aboufoul, T.; Alomainy, A.; Parini, C. Reconfiguring UWB Monopole Antenna for Cognitive Radio Applications Using GaAs FET Switches. *IEEE Antennas Wirel. Propag. Lett.* **2012**, *11*, 392–394. [CrossRef]
7. Akowuah, Y.B.; Tchao, E.T.; Ur-Rehman, M.; Khan, M.M.; Ahmad, S. Study of a Printed Split-Ring Monopole for Dual-Spectrum Communications. *Heliyon* **2021**, *7*, e07928. [CrossRef]
8. Khidre, A.; Yang, F.; Elsherbeni, A.Z. A Patch Antenna with a Varactor-Loaded Slot for Reconfigurable Dual-Band Operation. *IEEE Trans. Antennas Propag.* **2015**, *63*, 755–760. [CrossRef]

9. Ahmad, I.; Ullah, S.; Ullah, S.; Habib, U.; Ahmad, S.; Ghaffar, A.; Alibakhshikenari, M.; Khan, S.; Limiti, E. Design and Analysis of a Photonic Crystal Based Planar Antenna for THz Applications. *Electronics* **2021**, *10*, 1941. [CrossRef]
10. Sheikh, Y.A.; Paracha, K.N.; Ahmad, S.; Bhatti, A.R.; Butt, A.D.; Rahim, S.K.A. Analysis of the compact CP/LP Patch antenna design for wearable application. *Arab. J. Sci. Eng.* **2021**, *1*, 1–18.
11. Ghaffar, A.; Awan, W.A.; Hussain, N.; Ahmad, S.; Li, X.J. A Compact SIW-based Flexible Antenna for Applications at 900 and 2450 MHz. *Electromagn. Waves (Camb.)* **2021**, *99*, 83–91.
12. Nikolaou, S.; Bairavasubramanian, R.; Lugo, C.; Carrasquillo, I.; Thompson, D.; Ponchak, G.; Papapolymerou, J.; Tentzeris, M. Pattern and Frequency Reconfigurable Annular Slot Antenna Using PIN Diodes. *IEEE Trans. Antennas Propag.* **2006**, *54*, 439–448. [CrossRef]
13. Ahmad, S.; Ghaffar, A.; Hussain, N.; Kim, N. Compact Dual-Band Antenna with Paired L-Shape Slots for On- and Off-Body Wireless Communication. *Sensors* **2021**, *21*, 7953. [CrossRef] [PubMed]
14. Liang, C.; Li, L.; Zhai, H. Variational Stability Form for the Capacitance of an Arbitrarily Shaped Conducting Plate. *Chin. J. Electron.* **2004**, *13*, 714–718.
15. Ghosh, S.; Lim, S.A. Multifunctional Reconfigurable Frequency-Selective Surface Using Liquid-Metal Alloy. *IEEE Trans. Antennas Propag.* **2018**, *66*, 4953–4957. [CrossRef]
16. Gough, R.C.; Morishita, A.M.; Dang, J.H.; Hu, W.; Shiroma, W.A.; Ohta, A.T. Continuous Electrowetting of Non-toxic Liquid Metal for RF Applications. *IEEE Access* **2014**, *2*, 874–882. [CrossRef]
17. Entesari, K.; Saghati, A.P. Saghati, Fluidics in Microwave Components. *IEEE Microw. Mag.* **2016**, *17*, 50–75. [CrossRef]
18. Wang, Y.; Yoon, K.-C.; Lee, J.-C. A Frequency Tunable Double Band-Stop Resonator with Voltage Control by Varactor Diodes. *J. Electromagn. Eng. Sci.* **2016**, *16*, 159–163. [CrossRef]
19. Brown, M.; Saavedra, C.E. Tunable Branchline Coupler Using Microfluidic Channels. *IEEE Microw. Wirel. Compon. Lett.* **2019**, *29*, 207–209. [CrossRef]
20. Jiang, D.; Huang, T.; Shao, Z. Research of Nematic Liquid Crystal Broadband tunable power divider. In Proceedings of the 2014 IEEE International Conference on Communiction Problem-Solving, Beijing, China, 5–7 December 2014.
21. AliyuBabale, S.; Lawan, S.H.; IfeomaOrakwue, S.; Abdul Rahim, S.K. Implementation of 4 × 4 butler matrix using silver-nono instant inkjet printing technology. In Proceedings of the IEEE 3rd International Conference on Electro-Technology for National Development (NIGERCON), Owerri, Nigeria, 7–10 November 2017.
22. Qaroot, A.; Mumcu, G. Microfluidically Reconfigurable Reflection Phase Shifter. *IEEE Microw. Wirel. Compon. Lett.* **2018**, *28*, 684–686. [CrossRef]
23. Babale, S.A.; Rahim, S.K.; Barro, O.A.; Himdi, M.; Khalily, M. Single Layered 4 × 4 Butler Matrix without Phase-Shifters and Crossovers. *IEEE Access* **2018**, *6*, 77289–77298. [CrossRef]
24. Zaidi, A.M.; Beg, M.T.; Kanaujia, B.K.; Kishor, J.; Rambabu, K. A Novel Dual Band Branch Line Coupler and its Application to Design a Dual Band 4 × 4 Butler Matrix. *IEEE Access* **2020**, *8*, 65104–65115. [CrossRef]
25. Dong, Q.; Wu, Y.; Zheng, Y.; Wang, W.; Liu, Y. A Compact Single-Layer Ultra-Wideband Phase Shifter Using Weakly Coupled Lines. *IEEE Access* **2019**, *7*, 12575–12583. [CrossRef]
26. Babale, S.; Rahim, S.; Himdi, M.; Lawan, S.; Sani, F.; Usman, A. Implementation of inkjet-printed 3 dB coupler with equal power division and 45° output phase difference. *Microw. Opt. Technol. Lett.* **2020**, *63*, 1007–1011. [CrossRef]
27. Palomo, T.; Mumcu, G. Microfluidically Reconfigurable Microstrip Line Combline Filters with Wide Frequency Tuning Capabilities. *IEEE Trans. Microw. Theory Tech.* **2017**, *65*, 3561–3568. [CrossRef]
28. Kataria, T.K.; Osorio, L.; Cervantes, J.L.O.; Ayona, J.R.R.; Corona-Chavez, A. Microfluidic reconfigurable filter based on ring resonators. *Prog. Electromagn. Res.* **2018**, *79*, 59–63. [CrossRef]
29. Park, E.; Lim, D.; Lim, S. Dual-Band Band-Pass Filter with Fixed Low Band and Fluidically-Tunable High Band. *Sensors* **2017**, *17*, 1884. [CrossRef] [PubMed]
30. Babale, S.A.; Rahim, S.K.A.; Paracha, K.N.; Orakwue, S.I. 3 dB Branch-Line Coupler with Improved Bandwidth Using PDMS and Zoflex Conductor. *Adv. Sci. Lett.* **2017**, *23*, 11378–11381. [CrossRef]
31. Eom, S.; Memon, M.U.; Lim, S. Frequency-Switchable Microfluidic CSRR-Loaded QMSIW Band-Pass Filter Using a Liquid Metal Alloy. *Sensors* **2017**, *17*, 699. [CrossRef] [PubMed]
32. Abdallah, M.; Saavedra, C.E. Fluidically-tuned reflection oscillator at C-Band. In Proceedings of the 18th International Symposium on Antenna Technology and Applied Electromagnetics (ANTEM), Waterloo, ON, Canada, 19–22 August 2018.
33. Khan, S.; Vahabisani, N.; Daneshmand, M. A Fully 3-D Printed Waveguide and Its Application as Microfluidically Controlled Waveguide Switch. *IEEE Trans. Compon. Packag. Manuf. Technol.* **2017**, *7*, 70–80. [CrossRef]
34. Awang, R.A.; Baum, T.; Nasabi, M.; Sriram, S.; Rowe, W.S.T. Mechanically tolerant fluidic split ring resonators. *Smart Mater. Struct.* **2016**, *25*, 075023. [CrossRef]
35. Romero-Ramirez, M.-A.; Cervantes, J.L.O.; Kataria, T.K.; Corona-Chavez, A. Balanced Reconfigurable Filter Using Liquid Metal. *Prog. Electromagn. Res.* **2020**, *92*, 117–124. [CrossRef]
36. Diedhiou, D.L.; Sauleau, R.; Boriskin, A.V. Microfluidically tunable microstrip filters. *IEEE Trans. Microw. Theory Tech.* **2015**, *63*, 2245–2252. [CrossRef]
37. Gonzalez-Carvajal, E.; Mumcu, G. Frequency and Bandwidth Tunable Mm-Wave Hairpin Bandpass Filters Using Microfluidic Reconfiguration with Integrated Actuation. *IEEE Trans. Microw. Theory Tech.* **2020**, *68*, 3756–3768. [CrossRef]

38. Park, E.; Lee, M.; Lim, S. Switchable Bandpass/Bandstop Filter Using Liquid Metal Alloy as Fluidic Switch. *Sensors* **2019**, *19*, 1081. [CrossRef]
39. Dey, A.; Guldiken, R.; Mumcu, G. Microfluidically Reconfigured Wideband Frequency-Tunable Liquid-Metal Monopole Antenna. *IEEE Trans. Antennas Propag.* **2016**, *64*, 2572–2576. [CrossRef]
40. Murray, C.; Franklin, R.R. Independently Tunable Annular Slot Antenna Resonant Frequencies Using Fluids. *IEEE Antennas Wirel. Propag. Lett.* **2014**, *13*, 1449–1452. [CrossRef]
41. Paracha, K.N.; Butt, A.D.; Alghamdi, A.S.; Babale, S.A.; Soh, P.J. Liquid Metal Antennas: Materials, Fabrication and Applications. *Sensors* **2019**, *20*, 177. [CrossRef]
42. Lee, M.; Lim, S. Planar Inverted-F Antenna (PIFA) Using Microfluidic Impedance Tuner. *Sensors* **2018**, *18*, 3176. [CrossRef]
43. Morishita, A.M.; Dang, J.H.; Gough, R.C.; Ohta, A.T.; Shiroma, W.A. A tunable amplifier using reconfigurable liquid-metal double-stub tuners. In Proceedings of the Texas Symposium on Wireless and Microwave Circuits and Systems (WMCS), Waco, TX, USA, 23–24 April 2015.
44. Lei, B.J.; Hu, W.; Ohta, A.T.; Shiroma, W.A. A liquid-metal reconfigurable double-stub tuner. In Proceedings of the IEEE/MTT-S International Microwave Symposium Digest, Montreal, QC, Canada, 17–22 June 2012.
45. Song, L.; Gao, W.; Rahmat-Samii, Y. 3-D Printed Microfluidics Channelizing Liquid Metal for Multipolarization Reconfigurable Extended E-Shaped Patch Antenna. *IEEE Trans. Antennas Propag.* **2020**, *68*, 6867–6878. [CrossRef]
46. Song, L.; Gao, W.; Chui, C.O.; Rahmat-Samii, Y. Wideband Frequency Reconfigurable Patch Antenna with Switchable Slots Based on Liquid Metal and 3-D Printed Microfluidics. *IEEE Trans. Antennas Propag.* **2019**, *67*, 2886–2895. [CrossRef]
47. Borda-Fortuny, C.; Cai, L.; Tong, K.F.; Wong, K.-K. Low-Cost 3D-Printed Coupling-Fed Frequency Agile Fluidic Monopole Antenna System. *IEEE Access* **2019**, *7*, 95058–95064. [CrossRef]
48. Sun, J.; Luk, K. Miniature water monopolar patch antenna using transparent high-permittivity liquid substrate. *Electron. Lett.* **2020**, *56*, 475–476. [CrossRef]
49. Gonzalez, E.; Mumcu, G. Millimeter-Wave Beam-Steering Focal Plane Arrays with Microfluidically Switched Feed Networks. *IEEE Trans. Antennas Propag.* **2018**, *66*, 7424–7429. [CrossRef]
50. Gonzalez, E.; Mumcu, G. Integrated Actuation of Microfluidically Reconfigurable Mm-Wave SPST Switches. *IEEE Microw. Wirel. Compon. Lett.* **2019**, *29*, 541–544. [CrossRef]
51. Dey, A.; Mumcu, G. Microfluidically Controlled Frequency-Tunable Monopole Antenna for High-Power Applications. *IEEE Antennas Wirel. Propag. Lett.* **2016**, *15*, 226–229. [CrossRef]
52. Chen, C.-H.; Peroulis, D. Liquid RF MEMS Wideband Reflective and Absorptive Switches. *IEEE Trans. Microw. Theory Tech.* **2007**, *55*, 2919–2929. [CrossRef]
53. Wan, Z.; Zeng, H.; Feinerman, A. Reversible Electrowetting of Liquid-Metal Droplet. *J. Fluids Eng.* **2007**, *129*, 388–394. [CrossRef]
54. Armaroli, C.; Ferrario, L.; Giacomozzi, F.; Lorenzelli, L.; Margesin, B.T.; Rangra, K.; Tommaso, G. A silicon-based MEMS technology for electrostatically actuated SPDT RF switches. In Proceedings of the European Space Components Conference, ESCCON, Toulouse, France, 24–27 September 2002.
55. Moorefield, M.M.; Gough, R.C.; Dang, J.H.; Ohta, A.T.; Shiroma, W.A. A planar liquid-metal shunt switch. In Proceedings of the IEEE/ACES International Conference on Wireless Information Technology and Systems (ICWITS) and Applied Computational Electromagnetics (ACES), Honolulu, HI, USA, 13–18 March 2016.
56. Sanchez-Escuderos, D.; Ferrando-Bataller, M.; Baquero-Escudero, M.; Herranz, J.I. Reconfigurable Slot-Array Antenna With RF-MEMS. *IEEE Antennas Wirel. Propag. Lett.* **2011**, *10*, 721–725. [CrossRef]
57. González, E.; Mumcu, G. Microfluidic switches with integrated actuation for mm-wave beam-steering arrays. In Proceedings of the IEEE International Symposium on Antennas and Propagation and USNC-URSI Radio Science Meeting, Atlanta, GE, USA, 7–12 July 2019.
58. Mendoza, J.; Karabacak, M.; Arslan, H.; Mumcu, G. A Spatially Adaptive Antenna Array for Mm-Wave Wireless Channel Control with Microfluidics Based Reconfiguration. *IEEE Access* **2020**, *8*, 182898–182907. [CrossRef]
59. Yunusa, Z.; Hamidon, M.N.; Kaiser, A.; Awang, Z. Gas Sensors: A Review. *Sens. Transducers* **2019**, *168*, 61–75.
60. Li, F.; Zheng, Y.; Hua, C.; Jian, J. Gas Sensing by Microwave Transduction: Review of Progress and Challenges. *Front. Mater.* **2019**, *6*, 101. [CrossRef]
61. Sayago, I.; Fernández, M.; Fontecha, J.; Horrillo, M.; Vera, C.; Obieta, I.; Bustero, I. New sensitive layers for surface acoustic wave gas sensors based on polymer and carbon nanotube composites. *Sens. Actuators B Chem.* **2012**, *175*, 67–72. [CrossRef]
62. Phan, D.-T.; Chung, G.-S. Surface acoustic wave hydrogen sensors based on ZnO nanoparticles incorporated with a Pt catalyst. *Sens. Actuators B Chem.* **2012**, *161*, 341–348. [CrossRef]
63. Penza, M.; Rossi, R.M.; Alvisi, M.; Aversa, P.; Cassano, G.B.; Suriano, D.; Benetti, M.; Cannata', D.; Di Pietrantonio, F.; Verona, E. SAW Gas Sensors with Carbon Nanotubes Films. *IEEE Ultrason. Symp.* **2008**, 1850–1853.
64. Viespe, C.; Grigoriu, C. Surface acoustic wave sensors with carbon nanotubes and SiO_2/Si nanoparticles-based nanocomposites for VOC detection. *Sens. Actuators B Chem.* **2010**, *147*, 43–47. [CrossRef]
65. Park, J.-K.; Kang, T.-G.; Kim, B.-H.; Lee, H.-J.; Choi, H.H.; Yook, J.-G. Real-time Humidity Sensor Based on Microwave Resonator Coupled with PEDOT: PSS Conducting Polymer Film. *Sci. Rep.* **2018**, *8*, 439. [CrossRef]
66. Wiltshire, B.D.; Zarifi, M.H. 3-D Printing Microfluidic Channels with Embedded Planar Microwave Resonators for RFID and Liquid Detection. *IEEE Microw. Wirel. Compon. Lett.* **2019**, *29*, 65–67. [CrossRef]

67. Bogner, A.; Steiner, C.; Walter, S.; Kita, J.; Hagen, G.; Moos, R. Planar Microstrip Ring Resonators for Microwave-Based Gas Sensing: Design Aspects and Initial Transducers for Humidity and Ammonia Sensing. *Sensors* **2017**, *17*, 2422. [CrossRef]
68. Velez, P.; Grenier, K.; Mata-Contreras, J.; Dubuc, D.; Martin, F. Highly-Sensitive Microwave Sensors Based on Open Complementary Split Ring Resonators (OCSRRs) for Dielectric Characterization and Solute Concentration Measurement in Liquids. *IEEE Access* **2018**, *6*, 48324–48338. [CrossRef]
69. Bailly, G.; Harrabi, A.; Rossignol, J.; Michel, M.; Stuerga, D.; Pribetich, P. Microstrip Spiral Resonator for Microwave-Based Gas Sensing. *IEEE Sens. Lett.* **2017**, *1*, 1–4. [CrossRef]
70. Abduljabar, A.A.; Clark, N.; Lees, J.; Porch, A. Dual Mode Microwave Microfluidic Sensor for Temperature Variant Liquid Characterization. *IEEE Trans. Microw. Theory Tech.* **2017**, *65*, 2572–2582. [CrossRef]
71. Abdolrazzaghi, M.; Daneshmand, M.; Iyer, A.K. Strongly Enhanced Sensitivity in Planar Microwave Sensors Based on Metamaterial Coupling. *IEEE Trans. Microw. Theory Tech.* **2018**, *66*, 1843–1855. [CrossRef]
72. Yunusa, Z.; Hamidon, M.N.; Ismail, A.; Isa, M.M.; Yaacob, M.H.; Rahmanian, S.; Ibrahim, S.A.; Shabaneh, A.A. Development of a hydrogen gas sensor using a double SAW resonator system at room temperature. *Sensors* **2015**, *15*, 4749–4765. [CrossRef] [PubMed]
73. Bahoumina, P.; Hallil, H.; Lachaud, J.; Abdelghani, A.; Frigui, K.; Bila, S.; Baillargeat, D.; Ravichandran, A.; Coquet, P.; Paragua, C.; et al. Microwave flexible gas sensor based on polymer multi wall carbon nanotubes sensitive layer. *Sens. Actuators B Chem.* **2017**, *249*, 708–714. [CrossRef]
74. Bahoumina, P.; Hallil, H.; Lachaud, J.-L.; AbdelGhani, A.; Frigui, K.; Bila, S.; Baillargeat, D.; Zhang, Q.; Coquet, P.; Paragua, C.; et al. Chemical Gas Sensor Based on a Flexible Capacitive Microwave Transducer Associated with a Sensitive Carbon Composite Polymer Film. *Proceedings* **2017**, *1*, 439. [CrossRef]
75. Ali, M.A.; Cheng, M.M.C.; Chen, J.C.M.; Wu, C.T.M. Microwave gas sensor based on graphene-loaded substrate integrated waveguide cavity resonator. In Proceedings of the IEEE MTT-S International Microwave Symposium (IMS), San Francisco, CA, USA, 22–27 May 2016.
76. Ni, D.; Ravi, A.; Kumar, K.B.V.; Lal, A. A mechanically tunable GHz passive voltage element using microstrip resonator. *J. Phys. Conf. Ser.* **2019**, *1407*, 012051. [CrossRef]
77. Kim, H.K.; Lee, D.; Lim, S. A fluidically tunable metasurface absorber for flexible large-scale wireless ethanol sensor applications. *Sensors* **2016**, *16*, 1246. [CrossRef]
78. Salim, A.; Lim, S. Complementary split-ring resonator-loaded microfluidic ethanol chemical sensor. *Sensors* **2016**, *16*, 1802. [CrossRef]
79. Majhi, S.M.; Mirzaei, A.; Kim, H.W.; Kim, S.S.; Kim, T.W. Recent advances in energy-saving chemiresistive gas sensors: A review. *Nano Energy* **2021**, *79*, 105369. [CrossRef]
80. Kohl, D. Function and applications of gas sensors. *J. Phys. D Appl. Phys.* **2001**, *34*, 19. [CrossRef]
81. Nour, M.; Hussain, M. A Review of the Real-Time Monitoring of Fluid-Properties in Tubular Architectures for Industrial Applications. *Sensor* **2020**, *20*, 3907. [CrossRef] [PubMed]
82. Kwak, D.; Lei, Y.; Maric, R. Ammonia gas sensors: A comprehensive review. *Talanta* **2019**, *204*, 713–730. [CrossRef] [PubMed]